EVALUATION OF A STATIC AND DYNAMIC ROCKET THRUST MEASUREMENT TECHNIQUE

F. L. Crosswy and H. T. Kalb

ARO, Inc.

September 1968

ARNOLD ENGINEERING DEVELOPMENT CENTER
AIR FORCE SYSTEMS COMMAND
ARNOLD AIR FORCE STATION, TENNESSEE

NOTICES

When U. S. Government drawings specifications, or other data are used for any purpose other than a definitely related Government procurement operation, the Government thereby incurs no responsibility nor any obligation whatsoever, and the fact that the Government may have formulated, furnished, or in any way supplied the said drawings, specifications, or other data, is not to be regarded by implication or otherwise, or in any manner licensing the holder or any other person or corporation, or conveying any rights or permission to manufacture, use, or sell any patented invention that may in any way be related thereto.

Qualified users may obtain copies of this report from the Defense Documentation Center.

References to named commercial products in this report are not to be considered in any sense as an endorsement of the product by the United States Air Force or the Government.

EVALUATION OF A STATIC AND DYNAMIC ROCKET THRUST MEASUREMENT TECHNIQUE

F. L. Crosswy and H. T. Kalb
ARO, Inc.

AF -- AEDC
Arnold AFS Tenn

FOREWORD

The work presented herein was sponsored by Arnold Engineering Development Center (AEDC), Air Force Systems Command (AFSC), Arnold Air Force Station, Tennessee, under Program Element 62302F, Project 5730, Task 573004.

The results of the work were obtained by ARO, Inc. (a subsidiary of Sverdrup & Parcel and Associates, Inc.), contract operator of AEDC, AFSC, under Contract F40600-69-C-0001. The research and testing were performed from April to June, 1967, under ARO Project No. BC5703, and the manuscript was submitted for publication on May 6, 1968.

This technical report has been reviewed and is approved.

Forrest B. Smith, Jr.
Research Division
Directorate of Plans
and Technology

Edward R. Feicht
Colonel, USAF
Director of Plans
and Technology

ABSTRACT

This report describes the procedures and results of a critical evaluation of a static and dynamic rocket thrust measurement technique. A single-axis, experimental thrust stand was fabricated for the evaluation. When dynamically excited, the thrust stand exhibited three appreciable amplitude resonant or natural frequencies (393, 1670, and 3700 Hz). The thrust stand force measurement components were statically calibrated with a deadweight calibrator. The deadweight calibrator was also used to calibrate an electrodynamic actuator, which subsequently was used as a dynamic force calibrator. The dynamic force calibrator was used to excite the stand with variable frequency sinusoidal forces. The frequency domain, flat response bandwidth, of the load cell signal (typical of the conventional thrust stand output signal) was from 0 to 80 Hz. Two independent dynamic compensation techniques (reaction force summation and computer compensation techniques) were used in a "hybrid" tandem configuration to eliminate the force measurement signal distortions caused by the resonant frequencies. The compensated, flat response, bandwidth was extended to 1300 Hz, a factor of 16 improvement over the conventional load cell force measurement system. The dynamic force calibrator was also used to excite the stand with force-time functions approximating rocket thrust buildup, burn time, and tailoff. The resultant thrust stand natural frequency distortions were eliminated by using the hybrid compensation techniques. The time domain force measurement accuracy using hybrid compensation techniques was shown to be superior to that of the conventional load cell system. The general applicability of dynamic compensation techniques to first-(e.g., temperature sensors and anemometers), second-(e.g., pressure transducers), and higher-order dynamic measurement systems is also discussed.

CONTENTS

APPENDIXES

I. ILLUSTRATIONS

Figure

SECTION I
INTRODUCTION

The static rocket thrust force measurement problem can be solved in a straightforward manner by utilizing conventional ground test thrust stands with a load cell as the force transducer. However, the thrust forces produced by most solid- and liquid-propellant rockets are dynamic in nature, and the transient response characteristics of conventional thrust stands can cause distortion of the load cell signal. Conventional test data from a short burn-time, solid-propellant, rocket motor firing are shown in Fig. 1 (Appendix I). In this particular case, the transient response of the thrust stand structure persists throughout the entire test, and the resultant distortion of the load cell signal is evident. In general, static thrust stands and conventional data reduction techniques are not adequate to perform accurate dynamic thrust measurements. Accurate dynamic thrust measurements require the development of somewhat unconventional thrust stands and/or data recording and reduction techniques.

The ground test dynamic thrust measurement problem includes the static measurement problem as a special case. The accuracies of both static and dynamic thrust force measurements are affected by the following conventional thrust stand measurement error factors:

1. Hysteresis
2. Initial alignment
3. Deflection under load
4. Redundancy of force restraint
5. Pendulum effects
6. Temperature effects

The dynamic thrust measurement system must include both a dynamic-force calibrator and a conventional static (deadweight)-force calibrator to determine measurement system accuracy and precision. A dynamic force measurement system must possess the unconventional capability of furnishing a measurement signal that is an accurately scaled, undistorted, time-function replica of the thrust function in spite of the transient response characteristics of the thruster-thrust stand structure.

The solution of the dynamic thrust measurement problem requires a measurement system that produces an electrical analog signal with an

instantaneous tracking error percentage as small as possible. This percentage is defined as[1]

$$\frac{(\text{Actual Thrust Force} - \text{Measurement System Indicated Thrust Force}) \times 100 \text{ percent}}{\text{Actual Thrust Force}}$$

Several techniques have previously been proposed to produce a thrust measurement system with a small instantaneous tracking error percentage (Refs. 1 to 6). The "hybrid" combination of the reaction-force summation (accelerometer compensation) and analog computer compensation techniques was proposed (Ref. 6) as a particularly attractive approach to the dynamic thrust measurement problem. The object of this report is to critically evaluate the hybrid system dynamic- and static-force measurement characteristics.

To determine the validity and accuracy of a particular dynamic thrust measurement technique, the measurement system output signal must be compared with an analog signal representative of a known dynamic input force. This comparison is the essence of the dynamic-force calibration procedure. An electrodynamic actuator was used as the dynamic-force calibrator to evaluate the hybrid measurement system.

The first step in the evaluation procedure was to calibrate the electrodynamic actuator with a deadweight static-force calibrator. The hybrid system was next calibrated with the same deadweight calibrator. The actuator was then used as a transfer force standard to excite the thrust stand structure with dynamic and static forces. The actuator was then used to excite the stand with variable frequency sinusoidal forces to compare the frequency domain response characteristics of the stand, used in a conventional manner, with the stand characteristics when hybrid compensation techniques were employed. A current function generator was next used in conjunction with the actuator to excite the thrust stand structure with a dynamic force which approximated a rocket thrust function. The instantaneous tracking error characteristics of the hybrid system were then determined by oscilloscope presentation and comparison of the actuator force analog signal with the hybrid system force measurement signal.

---

[1]The terms "tracking error" and "instantaneous tracking error" will be used in general discussions of the overall dynamic force measurement accuracy characteristics of a certain thrust measurement system. The more formal term "instantaneous tracking error percentage" will be used when discussing force measurement accuracy of a certain thrust measurement system at a particular instant of time after initiation of a dynamic input force.

SECTION II
APPARATUS

2.1 EXPERIMENTAL THRUST STAND

The single-axis experimental thrust stand used to evaluate the hybrid thrust measurement technique and the electrodynamic actuator dynamic-force calibrator is schematically shown in Fig. 2. The force column of the stand consists of the armature of an electrodynamic actuator, an accelerometer housing, and a thrust-butt-mounted load cell. Static dead-weight calibration forces are imparted to the force column with a cable and low-friction bearing assembly.

2.2 ELECTRODYNAMIC ACTUATOR

An electrodynamic actuator was used to impart static and dynamic forces to the force column of the thrust stand. The actuator output force is given by

$$\bar{F}(t) = n\, I(t)\, \bar{L} \times \bar{B} \qquad (1)$$

where $\bar{F}(t)$ is the time-dependent, actuator force vector; $I(t)$ is the time-dependent armature current; $\bar{L}$ is the spatial orientation of the armature coils; n is the number of armature coils; and $\bar{B}$ is the vector field strength of the actuator magnetic field. From Eq. (1) it can be seen that for a constant magnetic field strength and constant cross product, $\bar{L} \times \bar{B}$, the actuator output force is directly proportional to, and in phase with, the armature current.

A variable amplitude, variable rise and fall time current function generator is used to drive the actuator armature. The current function generator can be programmed to produce a force-time function approximating rocket thrust rise time, burn time, and tailoff. A block diagram of the current function generator and electrodynamic actuator is shown in Fig. 3. A low ohmic resistance current shunt, fabricated with a metal alloy having a low-temperature coefficient of resistivity (Manganin®), is included in the armature electrical circuit to produce a voltage proportional to armature current. The current shunt is constructed to minimize inductive voltage drops during periods of rapidly changing armature currents. The inductance of the shunt is 0.15 μh, and inductive voltage drops are a small percentage of the shunt signal. Typical waveforms taken from the current shunt are shown in Fig. 4, which illustrates the variable rise and fall time capabilities of the current function generator. This generator

is capable of producing preselected linear current rise times from 0.5 to 20 msec, constant level current flow from 25 to 300 msec, and current fall times from 0.6 to 20 msec. The maximum current amplitude is variable from 0 to 12 amp, giving a peak force range from 0 to 75 lb.

Fast rise and/or fall time forces produced by the actuator excite the natural frequencies of the force column. These natural frequency distortions appear in the load cell signal and are then eliminated by proper adjustment of the electronic circuits of the hybrid force measurement system. Simultaneous oscilloscope presentation of the actuator force analog signal (the current shunt voltage) and the hybrid force measurement system signal permits a direct evaluation of the instantaneous tracking error characteristics of the thrust measurement system.

Abrupt current changes in the actuator armature electrical circuit produce an appreciable inductive voltage drop in the armature circuit and induce an appreciable voltage in the static magnetic field electrical circuit. Motion of the armature coils with respect to the static magnetic field generates a back electromotive force. These phenomena oppose the desired control of the actuator armature current by the function generator. However, the differential error control amplifier of the function generator possesses sufficient response characteristics to perform high-speed corrections so that precisely controlled armature currents are obtained. Induced voltages produced in the magnetic field coils because of changing armature currents can result in appreciable field currents which distort the desired force-time function. The effects of these induced voltages are practically eliminated by current control circuitry similar to that used for armature current control and by operation of the static magnetic field in the saturation region of its magnetization characteristic.

Precise control of the armature and magnetic field currents is accompanied by several somewhat undesirable features. The circuitry necessary to maintain precise control of these currents is moderately complex, but a more undesirable feature is dissipation of mechanical energy caused by the armature current control circuitry. With the force column at rest, the initial energy required to force current through the armature coils is totally furnished by the power supply of the current function generator. Subsequent vibratory motion of the armature coils with respect to the static magnetic field results in the availability of electrical energy because of the mechanical motion. Part of the total electrical energy required to produce the desired force is now furnished by the motion of the force column. This series of events results in dissipation of mechanical energy or damping. Electronic compensation adjustments are set into the hybrid force measurement system on the

basis of force column motions under the influence of the force and damping conditions dictated by the electrodynamic actuator. Experience has shown that the effect of the damping action of the actuator is small but not negligible. The damping ratio associated with the first mode natural frequency of the system shown in Fig. 2 is 0.004 during free vibration of the force column, whereas it is about 0.018 when the motion is damped by the actuator. (The damping effects of the actuator are discussed in Section 4.3.)

The actuator can also be driven with sinusoidal current waveforms. This allows determination of the dynamic response characteristics of the thrust measurement system in the frequency domain.

2.3 FORCE MEASUREMENT SYSTEM INSTRUMENTATION

A functional block diagram of the hybrid, static and dynamic, force measurement system is shown in Fig. 5. The basic transducer is a conventional load cell with a maximum force rating of 500 lb. Load cell electrical excitation is furnished by a conventional voltage-regulated power supply. The accelerometer is an undamped piezoelectric type with a mounted resonant frequency of 27 kHz. The accelerometer signal is fed to a conventional charge amplifier, which in turn furnishes one input signal to the summing amplifier. The load cell signal furnishes the other signal to the summing amplifier. The output of the summing amplifier furnishes the input signal to the linear phase filter, a Bessel type, with a variable cutoff frequency (100 to 10,000 Hz) and an attenutation rate of 18 db per octave. The computer compensator is an approximate differentiator type (Ref. 6) with a natural-frequency compensating range from 20 to 2000 Hz and a damping ratio compensating range from 0 to 1.0. The differential amplifiers and the summing amplifier are formed from conventional operational amplifiers with a unity gain-bandwidth product of 2 MHz. The digital voltmeter has an ultimate resolution of 1 mv. The null indicating voltage standard has an ultimate resolution of 20 μv.

2.4 STATIC-FORCE CALIBRATOR

The deadweight force calibrator was used to statically calibrate both the electrodynamic actuator and the hybrid force measurement system. The spatial orientation of the deadweight calibrator pull cable is coincident with the axis of the actuator armature to within ±0.001 in. This orientation precision was obtained with optical alignment equipment used during installation of the actuator and the deadweight calibrator. The in-place deadweight calibration of the load cell and the rest of the hybrid measurement circuitry obviates potentially inaccurate force measurements caused

by misalignment of the thrust-butt-mounted load cell and the rest of the force column. The weights of the steel calibration plates were determined by a precision beam balance to within ±1 gm.

SECTION III
PROCEDURE

3.1 STATIC-FORCE CALIBRATION OF THE ELECTRODYNAMIC ACTUATOR AND THE HYBRID FORCE MEASUREMENT SYSTEM

The actuator magnetic field current was set to 1.75 amp. Deadweight of 14,128 gm was placed on the static-force calibrator cable. Next, a d-c power supply was used to increase the current in the actuator armature (Fig. 3) until no net force was imparted to the load cell, as indicated by the null indicating voltage standard (Fig. 5). At this point in the calibration procedure, the developed force of the actuator just balanced the deadweight force. The voltage developed across the armature shunt, as indicated by digital voltmeter No. 1 (Fig. 3), was recorded as an actuator calibration point. The d-c power supply was then disconnected, and the gain of the summing amplifier (Fig. 5) was adjusted until the reading of digital voltmeter No. 2 was identical to the previous reading of digital voltmeter No. 1. This procedure caused the hybrid force measurement system scale factor (lb_f/v) to be equal to the actuator scale factor (lb_f/v). Equal scale factors permit direct determination of the instantaneous tracking error characteristics of the measurement system. Tracking error is determined by direct comparison of the voltage signal across the armature shunt (armature current function determined by the current function generator) with that at the output of the hybrid measurement system.

The deadweights were next increased in ten increments from 0 to 28,128 gm, and the calibration points for the actuator were determined with the d-c power supply operative (whereas the static calibration points of the hybrid system were determined with the power supply inoperative).

3.1.1 Systematic Errors and Accuracy

The calibration voltages of the actuator and hybrid system were determined with digital voltmeters. The systematic error caused by digital voltmeter calibration errors was eliminated by frequent use of the internal calibration voltage standards of these particular voltmeters. The systematic error caused by temperature-dependent changes of shunt resistance was minimized by using a metal alloy with a low-temperature coefficient of resistivity (Manganin).

The first static-force calibration plot for the actuator showed that an appreciable systematic error was caused by static friction effects in the calibrator cable bearing (Fig. 2). This error was apparent since the first two calibration points fell far below the straight line determined by the next four calibration points. The calibration procedure was repeated, and the error was eliminated by imparting a dither excitation (light impact forces) to the stand while recording each calibration point. The static-force calibration procedure (with dither excitation) then was repeated a third time by another observer. The results of the third calibration were practically identical to those obtained in the second calibration. The precisely linear relationship and random scatter of the 11 actuator calibration points indicated that the effects of systematic errors were small and, therefore, the static force of the actuator could be determined with high accuracy.

It was recognized that dynamic actuator forces could not be determined as accurately as static forces since inductive as well as resistive voltage drops would appear across the shunt when the actuator armature current was changing rapidly. However, the current shunt was geometrically fabricated to minimize its inductance. The inductance of the shunt is 0.15 μh and the maximum inductive voltage drop for a 0.6-msec rise time, 50-lb peak actuator force is about 0.002 v, or approximately 0.25 percent of the peak shunt voltage.

The systematic static-force measurement errors of the hybrid system were also found to be quite small as revealed by static deadweight calibration.

The force measurement accuracy of the hybrid system for dynamic forces is analyzed and discussed in detail in Section IV.

The dynamic data recording technique, oscilloscope photographs, used to record the dynamic actuator force and the hybrid measurement system signal resulted in an appreciable resolution error. It was determined that the oscilloscope data could be "read" with a resolution error no better than ±1.3 percent of the full-scale oscilloscope presentation. However, the use of a digital sampling data recording system could reduce this error to less than 1 percent of the actual value to be recorded.

3.1.2 Random Errors and Precision

A statistical sample of eight readings was obtained at each of the static calibration points so that the precision involved in determining the actuator force and the hybrid system measurements could be defined. The weights of the steel calibration plates were determined to within

1 gm by using a precision beam balance. The plate weights were therefore considered exact, and the random errors were considered to be concentrated in the shunt voltage signal and the hybrid system signal.

The most probable value of a measured quantity is just the arithmetic average of the individual measurements (Ref. 7)

$$\bar{y} = \frac{\sum_{n=1}^{k} y_n}{k} \tag{2}$$

where $\bar{y}$ is the arithmetic average, y_n is a measured value, and k is the total number of measurements. The precision of the k measurements is represented by the standard deviation

$$s = \left(\frac{\sum_{n=1}^{k} (\delta y_n)^2}{k-1} \right)^{1/2} \tag{3}$$

where s is the standard deviation and δy_n is the deviation of the nth measurement from the arithmetic average.

The width of the confidence interval, d, for each data point is given by (Ref. 8)

$$d = \frac{2t_{\alpha/2(n-1)}\, s}{(k)^{1/2}} \tag{4}$$

where t is a particular value from the t-sampling distribution tables and α is the desired confidence interval percentage.

3.2 FREQUENCY DOMAIN CHARACTERISTICS OF THE HYBRID FORCE MEASUREMENT SYSTEM

Several sets of frequency response data were recorded to determine the validity of using hybrid compensation techniques. The results reveal that the frequency response bandwidth of a conventional thrust stand could be appreciably extended by use of the hybrid techniques. The following data were recorded: (1) the acceleration transmissibility (normalized to the value at 160 Hz) to identify the predominant amplitude resonant frequencies, (2) the force transmissibility (normalized to the value at 5 Hz) of the load cell signal to illustrate the conventional thrust stand response, (3) the indicated force transmissibility (normalized to the value at 5 Hz) of the reaction-force summation technique (accelerometer compensation) to show an improved response as compared with the conventional thrust stand response, and (4) the hybrid system indicated force transmissibility (normalized to the value at 5 Hz) to illustrate the comparative performance of the conventional, the reaction-force summation, and hybrid system responses.

The electrodynamic actuator was used to excite the stand structure with variable frequency sinusoidal forces so that the frequency response data could be recorded.

3.3 TIME DOMAIN CHARACTERISTICS OF THE HYBRID FORCE MEASUREMENT SYSTEM - DYNAMIC-FORCE CALIBRATION

The current function generator was programmed to drive the actuator armature with a current function similar to that shown in Fig. 4b. This current function was displayed on an oscilloscope, and the corresponding force at any instant of time could be determined from the previous deadweight calibration. A chopped input vertical amplifier (chopper frequency = 1 MHz) was used with the oscilloscope so that the actuator current shunt signal and the hybrid measurement signal could be displayed simultaneously. The particular deadweight calibration procedure employed in this study caused the actuator calibration scale factor

$$\left(\frac{\text{lbf output}}{\text{volts developed across the shunt}}\right)$$

to be equal to the hybrid measurement system scale factor

$$\left(\frac{\text{lbf measured}}{\text{volts output}}\right)$$

The chopped input oscilloscope presentation and equal scale factors permitted the instantaneous tracking error characteristics of the hybrid system to be recorded directly from oscilloscope photographs.

A series of oscilloscope photographs illustrated the progressively improved time domain response as the components of the hybrid system were successively added to the conventional thrust measurement system.

The effectiveness of the successive compensation stages of the hybrid system was determined by comparing the magnitude of the instantaneous tracking error percentages which resulted after each stage was introduced. Other error criteria, such as the average mean squared error, could also be used to evaluate measurement effectiveness, but it is obvious that if the instantaneous tracking error percentage is a minimum for each instant of time, any practical error criteria must also be a minimum. The instantaneous tracking error percentage is therefore considered to be a straightforward and basic criterion for the evaluation of a dynamic-force measurement system.

SECTION IV
RESULTS AND DISCUSSION

4.1 STATIC-FORCE CALIBRATION OF THE ELECTRODYNAMIC ACTUATOR AND THE HYBRID FORCE MEASUREMENT SYSTEM

The electrodynamic actuator and the hybrid measurement system were statically calibrated according to the procedures set forth in Section III.

4.1.1 Static Calibration of the Electrodynamic Actuator

A statistical sample of eight readings was recorded for each of the first six calibration points. Only one reading was recorded for each of the next five points because the excessive armature currents required caused overheating of the armature coils.

The static-force calibration data for the electrodynamic actuator are shown in Table I (Appendix II). The small values of standard deviation (Eq. 3) and 95-percent confidence interval (Eq. 4) obtained for each of the first six calibration points show that the actuator was precisely calibrated. The standard deviations of the statistically sampled calibration points do not vary greatly from one point to the next, and it is estimated that the standard deviation and 95-percent confidence interval associated with each of the single reading calibration points are no greater than 2×10^{-3} and 3.5×10^{-3} v, respectively. Therefore, it is estimated that the static force developed by the actuator at the 50-lb level is determinable to within 0.4 percent (95-percent confidence) of the actual value.

The actuator calibration data are shown in graphical from in Fig. 6. The vertical line at each of the first six calibration points is equal in magnitude to the calculated 95-percent confidence intervals.

The drift characteristics of the d-c power supply used in the actuator calibration procedure were found to cause the largest percentage of the random error. The supply was not current regulated so it was necessary to continually adjust the current level. The continually changing current, in turn, caused a small changing force which directly affected the load cell signal. It was planned to record an actuator calibration data point when the null indicating voltage standard (Fig. 5) indicated that no force was acting on the load cell. However, the constantly changing force level resulted in recording the "best estimate" readings of the load cell null position. The use of a current-regulated power supply could significantly

reduce the random error and standard deviations associated with the actuator calibration. Reducing the standard deviations would also reduce the widths of the 95-percent confidence intervals. The confidence intervals for the actuator and hybrid system calibrations were considered acceptable for the present study.

4.1.2 Static Calibration of the Hybrid System

The static-force calibration data for the hybrid measurement system are shown in Table II. The small values of the standard deviation and 95-percent confidence interval at each calibration point are indicative of the precision associated with the calibration procedure. Using the data of Table II, it can be statistically inferred that the hybrid system signal at the 50-lb static-force level determines this force to within 0.35 percent (95-percent confidence).

The random error in the calibration data was predominantly caused by drift of the differential and summing amplifiers (Fig. 5) which were not stabilized. The precision of the hybrid system could be improved somewhat by using stabilized amplifiers. Random error also was introduced by the drift characteristics of the charge amplifier, the Bessel filter, and the computer compensator circuitry. Again, reduced drift and improved precision could be realized only by the use of more expensive components.

The hybrid system static calibration data are shown graphically in Fig. 7. The vertical line at each of the calibration points is equal in magnitude to the 95-percent confidence interval at that point.

4.2 FREQUENCY DOMAIN CHARACTERISTICS OF THE HYBRID FORCE MEASUREMENT SYSTEM

The predominant amplitude resonant frequencies of the system shown in Fig. 2 were identified by the acceleration transmissibility plot shown in Fig. 8. These data were normalized to the transmissibility value at 160 Hz. From Fig. 8 it can be seen that the three major resonant frequencies occur at 393, 1670, and 3700 Hz. It can also be seen that the resonances are lightly damped so that the resonant frequencies are equal, for all practical purposes, to the time domain natural frequencies. The excitation of a resonant or natural frequency results in distortion of the force measurement signal in the frequency or time domain, respectively. The purpose of the electronic section of the hybrid system is to eliminate these distortions in such a way that the frequency domain measurement

bandwidth is increased and the time domain tracking errors are decreased.

The frequency domain plots of Figs. 9 through 11 show conclusively that hybrid measurement techniques can be used in a straightforward manner to eliminate the resonant frequency distortions.

The load cell force transmissibility data (normalized to the value at 5 Hz) are shown in Fig. 9. The distortion caused by the 393-Hz resonant frequency is evident. The distortion effects of the 1670-Hz resonant frequency are apparent also but are relatively unimportant in this case since the 393-Hz resonant frequency is the predominant distortion mechanism. This plot is typical of the conventional thrust stand. The flat response bandwidth of this system is only from 0 to 80 Hz, and the dynamic-force measurement capabilities are severely limited.

The proper summation of the load cell and accelerometer signals in the reaction-force summation (accelerometer compensation) configuration was next utilized to eliminate the 393-Hz resonant frequency distortion. The results of this first step in the hybrid compensation scheme are shown in Fig. 10. The improvement in the frequency response characteristic is evident. The flat response bandwidth has been increased by almost an order of magnitude over that of the conventional system response (Fig. 9). However, the distorting effects of the 1670- and 3700-Hz resonant frequencies have been amplified by the addition of the accelerometer signal. This was to be expected since the accelerometer signal is the second time derivative of the load cell signal and is, for sinusoidal excitations, greater than the load cell signal by a factor proportional to the square of the radian resonant frequency. When the reaction-force summation technique is used, it can always be expected that elimination of the first resonant frequency distortion will be obtained at the expense of distortion by the higher resonant frequencies. The equivalent time domain statement is that use of the reaction-force summation technique to reduce the tracking error caused by the first mode natural frequency will be accompanied by an increase in the tracking error caused by the higher mode natural frequencies.

It should be emphasized at this point that the application of the reaction-force summation technique to eliminate the first resonant frequency distortion of lightly damped thrust stand structures has a sound physical basis - Newton's third law of motion (Refs. 3, 4, and 6).

The second stage of the hybrid compensation scheme was next employed to eliminate the 1670-Hz distortion produced by the first compensation stage. This second compensation stage consists of approximate

differentiator-type operational amplifier circuitry and is referred to as an analog computer compensator. The results of using the computer compensator stage are shown in Fig. 11. The flat response bandwidth has now been increased to 1300 Hz. This represents a bandwidth increase of 16 over that of the conventional load cell response (Fig. 9). A second stage of computer compensation circuitry could have been used to reduce the distortion caused by the 3700-Hz resonant frequency. However, only one computer compensation stage was available at the time of this study.

The physical basis for the application of computer compensation techniques to linear systems is not as universally recognized as is Newton's third law for the reaction-force summation technique. but it is nevertheless based on sound theoretical considerations (Refs. 5 and 6). The computer compensator is simply programmed with the inverse transfer function of the thrust stand structure for one particular degree of freedom. The input force information is distorted by the thrust stand structural response characteristics, and the computer compensator, having been programmed with the inverse response characteristics of the stand structure, is able to reconstruct the actual force information.

Conventional filtering techniques are sometimes used to reduce the distortion caused by the natural-frequency response of thrust stand structures. Even a superficial frequency domain examination of filter characteristics shows that force information is lost when filter techniques are employed. Although filter techniques may greatly attenuate the natural-frequency distortion, it is evident that force information in the same frequency bandwidth as the natural frequencies is also greatly attenuated and the measurement frequency bandwidth is actually reduced. Therefore, compensation, rather than attenuation, techniques should be perfected to improve the frequency domain characteristics of a thrust measurement system.

Perusal of Figs. 9 through 11 shows conclusively that the frequency domain response characteristics of a thrust measurement system can be greatly improved by using hybrid compensation techniques.

4.3 TIME DOMAIN CHARACTERISTICS OF THE HYBRID FORCE MEASUREMENT SYSTEM - DYNAMIC-FORCE CALIBRATION

Dynamic-force calibration of the hybrid measurement system can be accomplished in the frequency domain, as shown in Figs. 9 through 11. However, this process is extremely tedious and time consuming. On the other hand, dynamic-force calibration in the time domain is quite straightforward and requires only about two minutes for the system shown in Fig. 2.

The force-time function shown in Fig. 12a was programmed into the current function generator and electrodynamic actuator. This particular force-time function simulates a rocket thrust force buildup, constant-level duration, and tailoff. The force at any instant of time was determined from the previous static-force calibration of the electrodynamic actuator. The largest error involved in determining the dynamic force at any instant is caused by the "readability" of the oscilloscope photographs. It was determined that these can be "read" with a resolution error no better than 1.3 percent of the full-scale oscilloscope presentation. This error, combined with the random error associated with the calibration of the actuator and the error caused by inductive voltage drops across the current shunt, permits a determination of the actual force to within about 2 percent of the actual force at the 50-lb level. A more precise calibration procedure (using a current-regulated power supply) and use of digital sampling data recording procedures should permit determination of the actual force to less than 1 percent of the actual value. However, the time-function specification of the dynamic force would be limited by the sampling rate of the digital sampler. All subsequent values quoted for the force generated by the electrodynamic actuator are to be interpreted as accurate to within about 2 percent of the quoted value.

The experimental thrust stand was repetitively excited with the force-time function shown in Fig. 12a. By using the chopped input oscilloscope amplifier, the load cell signal was superimposed upon the dynamic-force signal, as shown in Fig. 12b. This load cell signal is typical of conventional thrust stand signals, and the instantaneous tracking error percentages are obviously quite large. An expanded time scale photograph of Fig. 12b is shown in Fig. 12c.

The next step in the dynamic-force calibration procedure was to employ the reaction-force summation technique to eliminate the 393-Hz distortion (Figs. 12b and c). The result of the proper summation of the load cell and accelerometer signals is shown in Fig. 12d. An expanded time scale photograph of Fig. 12d is shown in Fig. 12e. From Figs. 12d and e it can be seen that the 393-Hz distortion has been practically eliminated and that the 1670-Hz natural frequency now distorts the measurement signal. The summation signal can be seen to "track" the calibration force signal much more closely than the measurement signal shown in Figs. 12b and c. It is important to note that use of the reaction-force summation technique has resulted in a noticeable reduction of tracking error during the rise time portion of the calibration force, as well as practically eliminating the 393-Hz "ringing" distortion. This would not be the case if conventional filtering techniques had been used to reduce the 393-Hz ringing distortion. A filter cutoff frequency obviously could be chosen to eliminate the ringing distortion, but the use of the filter

would cause the tracking error during the rise time portion of the calibration force to be greater than that associated with the original load cell signal.

Perusal of Figs. 12d and e shows that the 393-Hz ringing distortion has not been completely eliminated. The damping action of the electrodynamic actuator, discussed in Section 2.2, causes the residual distortion. The damping action causes the phase of the load cell signal with respect to the accelerometer signal to be slightly different from the ideal 180 deg.

The computer compensator can also be used to compensate for the 393-Hz distortion of the load cell signal. The computer-compensated signal is shown in Fig. 12f. An expanded time scale photograph of Fig. 12f is shown in Fig. 12g. Comparison of Figs. 12f and g with Figs. 12d and e shows that the tracking error characteristics of the computer-compensated signal during the calibration force rise time are slightly inferior to those of the reaction-force summation signal. The lagging response of the computer-compensated signal is caused by the noise filter, which must be used with the computer circuitry. The filter cutoff frequency was set at 6 kHz. As previously stated, it is not desirable to filter the load cell signal, but it was necessary in this case to attenuate high-frequency noise signals before introduction into the differentiator circuitry of the computer. The filter is a Bessel type with a maximally flat time delay characteristic (Ref. 6).

Observation of the computer-compensated signal in Fig. 12f shows that the 393-Hz distortion has been virtually eliminated, whereas a slight residual distortion remains in the reaction-force summation signal shown in Fig. 12d. The computer circuitry can easily be programmed to accommodate damping effects and is, therefore, superior to the basic reaction-force summation circuitry in this regard.

The final step in the dynamic-force calibration procedure was to form a hybrid combination of the reaction-force summation circuitry and computer compensation circuitry, making it possible to compensate for the 393- and 1670-Hz structural natural frequencies. The reaction-force summation circuitry was used to compensate for the 393-Hz natural-frequency response, and the computer compensator for the 1670-Hz natural-frequency response. Thrust butt motions were not a problem during the entire study and, therefore, the quite valuable thrust butt motion insensitivity property of the reaction-force summation technique was not exploited. This insensitivity to thrust butt motions could be a significant asset for those thrust measurement problems in which the load cell signal is distorted by thrust butt motions caused by

dynamic thrust forces and/or test cell background vibrations (Refs. 4 and 6). Another stage of computer compensation could have been used to compensate for the 3700-Hz natural frequency, but was not available during this study.

The hybrid system signal superimposed on the actuator force-time function signal is shown in Fig. 12h. An expanded time scale photograph of Fig. 12h is shown in Fig. 12i. It can be seen that the force measurement signal now tracks the dynamic-force calibrator signal much more closely than the original load cell signal. The tracking error during the rise time portion of the calibrator signal is principally caused by the uncompensated 3700-Hz natural-frequency distortion, and could be reduced with another stage of computer circuitry. Also, the tracking error during the 3 msec following the rise time portion of the calibrator force is predominantly caused by the uncompensated 3700-Hz natural-frequency distortion.

The maximum tracking error 4 msec after the initiation of the calibrator force is about 3.5 percent and is caused by the imperfectly compensated 393-Hz natural-frequency distortion, several quite small amplitude natural frequencies 3700 Hz and higher, and random electronic noise. The largest part of the tracking error after 4 msec is caused by the 393-Hz residual distortion which, as explained earlier, is caused by the damping action of the dynamic-force calibrator (electrodynamic actuator.) The damping ratio associated with the 393-Hz natural frequency is 0.018 when the actuator is operative, but only 0.004 when it is inoperative. It is important to note that the electrodynamic actuator would be inoperative during an actual rocket firing, and the residual 393-Hz distortion would be almost negligible. The reaction-force summation circuitry would quite effectively eliminate the 393-Hz distortion for a damping ratio of 0.004. Elimination of the residual 393-Hz distortion would result in a maximum tracking error of about 2 percent 4 msec after the initiation of the rocket force (for a force-time function similar to that shown in Figs. 12h and i). This tracking error is about an order of magnitude greater than the random error associated with the static-force calibration of the hybrid system. For this particular study, the static-force calibration error makes a practically negligible contribution to the overall dynamic-force measurement error of the hybrid system.

It is anticipated that dynamic-force calibration of the hybrid system under actual test conditions would be carried out under the most severe

dynamic excitation conditions (fast rise time calibration forces) that could be furnished by the electrodynamic actuator. With the system calibrated under worst case conditions, less severe dynamic-force excitations could be accommodated with ease. For example, the data shown in Fig. 13 were recorded following the dynamic-force calibration procedure discussed above. From Fig. 13 it can be seen that the dynamic-force calibrator rise time (from 0 to 100 percent) is 5 msec, and the maximum force level is 48.97 lb (within 2 percent). The tracking error of the hybrid system is about 5 percent 1 msec after the initiation of the calibrator force, 2.5 percent at 3 msec, and virtually zero at 5 msec and thereafter.

Considering the preceding discussions and the data recorded in Figs. 12 and 13, it should be observed that the instantaneous tracking error characteristics of the three-degree-of-freedom thrust stand shown in Fig. 2 are directly influenced by the input force rise time and the effectiveness of the hybrid compensation technique. In general, compensation for three or possibly four degrees of freedom of any thruster-thrust stand structure is a practical limit for the hybrid compensation technique. Predominantly single-degree-of-freedom thruster-thrust stand structures such as shown in Fig. 14 (from Ref. 9) can be compensated easily and effectively, and the instantaneous tracking errors can be made quite small. In general, the effectiveness of the hybrid compensation technique is inversely proportional to the severity of the dynamic thrust excitation and the number of structural natural frequencies to be compensated.

SECTION V
SUMMARY OF RESULTS AND CONCLUSIONS

A deadweight static-force calibrator was used to accurately and precisely calibrate a dynamic-force calibrator (electrodynamic actuator) and a static- and dynamic-force measurement system (hybrid system). The static output force of the dynamic calibrator at the 16,388-gm (36.1-lb) level was determined within 0.33 percent (95-percent confidence) and at the 26-kg (57.26-lb) level the error was considered to be within 0.35 percent. Static forces could be determined to within 0.34 percent (95-percent confidence) at the 26-kg (57.26-lb) level when using the hybrid measurement system. The random errors associated with the static-force calibration of both the dynamic-force calibrator and the hybrid force measurement system could be reduced by using higher quality, more sophisticated components than those used in this study.

The developed force of the actuator was monitored by recording the voltage drop across a low-temperature coefficient of resistivity current shunt in the armature circuit. The static-force calibration of the actuator was valid when dynamic forces were generated since the current shunt was almost purely resistive. The error caused by inductive voltage drops across the shunt was only about 0.25 percent for a 0.6-msec rise time ramp force with a 26-kg (57.26-lb) peak force level. Oscilloscope photographs, used to record all time domain data, introduced a large, 1.3-percent oscilloscope resolution error into the determination of the dynamic forces (at the 57.26-lb level) produced by the electrodynamic actuator and measured by the hybrid system.

Considering the static calibration and oscilloscope resolution random errors and the systematic error caused by current shunt inductive voltage drops, the dynamic forces (at the 57.26-lb level) produced by the actuator were determined to within about 2 percent of the actual value. The use of higher quality components and high-speed, digital sampling data recording techniques should reduce this figure to less than 1 percent.

The actuator was used to excite the experimental thrust stand with sinusoidal forces. Frequency response plots were then made for the accelerometer signal (to identify the structural resonant frequencies), the load cell signal (to illustrate conventional thrust stand response), the reaction-force summation signal (to illustrate improved dynamic response) and, finally, the hybrid system signal (to illustrate optimum dynamic response). Appreciable amplitude resonant frequencies were recorded at 393, 1670, and 3700 Hz. The flat response bandwidth of the load cell force measurement system was determined to be from 0 to 80 Hz and that of the reaction-force summation system was determined to be from 0 to 650 Hz. The flat response bandwidth of the hybrid system was found to be from 0 to 1300 Hz, a factor of 16 improvement over the conventional load cell system. The availability of another stage of computer compensation would have made it possible to extend the bandwidth to about 3 kHz. Therefore, it was conclusively demonstrated that the frequency response characteristics of a single-axis, three-degree-of-freedom thrust stand could be significantly improved by using the hybrid compensation techniques.

The electrodynamic actuator was next used as a transfer force standard to introduce time domain dynamic calibration forces into the thrust stand structure. With the stand excited by repetitive dynamic calibration forces (0.8-msec rise time, 57.26-lb peak force), the time domain response characteristics of the force measurement system were

recorded. The load cell signal (typical of the conventional thrust stand signal) showed that 393-Hz natural-frequency distortion produced large instantaneous tracking errors. The reaction-force summation system signal revealed that the 393-Hz distortion was practically eliminated, but that the 1670-Hz natural-frequency distortion was amplified in the process. A hybrid combination of the reaction-force summation technique and the computer compensation technique was next employed to eliminate both the 393- and 1670-Hz distortions. An additional stage of computer circuitry could have been used to eliminate the 3700-Hz distortion. The instantaneous tracking error characteristics of the force measurement system resulting from the hybrid combination of the reaction-force summation technique and computer compensation technique were shown to be superior to those of either technique used individually. The tracking error characteristics of the hybrid system were shown to be much superior to those of the conventional load cell system. The entire dynamic-force calibration procedure from activation of the actuator and adjustment of the electronic compensator circuits through the recording of the data by an oscilloscope photograph required only about two minutes. The direct oscilloscope comparison of the hybrid system signal with the dynamic-force calibrator (electrodynamic actuator) signal conclusively demonstrated the validity and utility of the dynamic compensation techniques used.

A quite valuable asset of the reaction-force summation technique was not exploited during this study: the insensitivity of the reaction-force summation system to thrust butt motions. When the load cell and accelerometer signal gains are adjusted and summed to compensate for the first mode natural frequency of the thruster-thrust stand structure, the resultant summation signal is inherently insensitive to thrust butt motions, regardless of complexity. Therefore, thrust butt motions caused by dynamic thrust forces and/or test cell background vibrations do not distort the thrust measurement signal.

A practical thrust stand, optimally designed for dynamic as well as static thrust measurements, could be fabricated with a commercially available electrodynamic actuator as the dynamic-force calibrator.

Existing conventional thrust stands with essentially linear dynamic response characteristics could be modified to utilize hybrid force measurement techniques. This modification could appreciably reduce measurement signal distortions caused by thrust butt motions. The hybrid system with several computer compensator stages could eliminate distortions caused by as many as three or possibly four degrees of freedom of the thruster-thrust stand structure.

Existing conventional thrust stands could be readily modified to use the hybrid measurement technique, but the structural modifications to

incorporate a dynamic-force calibrator of the electrodynamic actuator type would require major mechanical modifications. However, a mechanically and electronically simple impact-type dynamic-force calibrator could conceivably be attached to an existing thrust stand. The impact-type force calibrator would consist of a high natural frequency load cell or dynamic-force gage which is set into motion and caused to impact upon a certain point on the thrust stand. The impacting force gage would produce a calibration signal representative of the dynamic impact force. The force gage would be calibrated with deadweight before installation on the thrust stand. The impact calibrator assembly would be mechanically aligned so that the impact force vector could be defined. The impact material (such as sheet rubber) attached to the thrust stand could be chosen so that the natural frequency of the force gage would not be excited. It is conceivable that one impact-type dynamic-force calibrator could be provided for each force component to be measured with a multicomponent thrust stand.

A conventional thrust stand is shown in Fig. 15a. This same stand is shown in Fig. 15b with modifications to accommodate the hybrid measurement technique and a single-axis, impact-type dynamic-force calibrator.

REFERENCES

1. Republic Aviation Division of Fairchild Hiller Corporation. "High Response, Low Level Thrust Stand System." Report No. FHR 2621-2, PCD-TR-65-25, Farmingdale, New York, October 1965.

2. Couvillion, A. J., Smith, J. D., and Kuberek, R. "High Response, Low Level Pulse Engine Thrust Stand System." AFRPL-TR-66-321, Hughes Research Laboratories, Malibu, California, December 1966.

3. Ward, J. S. "A System for Correcting for Spurious Natural Frequency Ringing of Rocket Thrust Stands." U. S. Naval Ordnance Test Station NOTS TP 2541, NAV WEPS 7569, China Lake, California, September 1960.

4. Postma, R. W. "Pulse Thrust Measuring Transducer." Rocketdyne Division of North American Aviation, Inc., Report No. R-6044, Canoga Park, California, January 1965.

5. Liu, F. F., and Berwin, T. W. "Extending Transducer Transient Response by Electronic Compensation for High-Speed Physical Measurements." The Review of Scientific Instruments, Vol. 29, No. 14-22, January 1958.

6. Crosswy, F. L. and Kalb, H. T. "Investigation of Dynamic Rocket Thrust Measurement Techniques." AEDC-TR-67-202 (AD823181), November 1967.

7. Beers, Y. Theory of Error. Addison-Wesley, Reading, Massachusetts, 1953.

8. Huntsberger, D. V. Elements of Statistical Inference. Allyn and Bacon, Inc., Boston, Massachusetts, 1961.

9. Smith, R. E., Jr. "Testing Techniques for Small Solid Rocket Motors at Simulated High Altitude Conditions." Joint Army-Navy-Air Force Solid-Propellant Rocket Static Test Panel, Paper No. 143, Palo Alto, California, October 1962.

10. Schwartz, M. Information Transmission, Modulation, and Noise. McGraw-Hill Book Company, New York, 1959.

11. Sprouse, J. A. and McGregor, W. K. "Investigations of Thrust Compensation Methods." AEDC-TDR-63-85 (AD411841), August 1963.

12. Lee, O. B. "The Analog Computer as a Compensator for Rocket Thrust Data." Master's Thesis, The University of Tennessee, Knoxville, Tennessee, 1965.

13. Shepard, C. E., and Warshawsky, I. "Electrical Techniques for Compensation of Thermal Time Lag of Thermocouples and Resistance Thermometer Elements." NACA Technical Note 2703, May 1952.

14. Kovasznay, L. S. G. "Development of Turbulence-Measuring Equipment." NACA Technical Note 2839, January 1953.

15. Edenfield, E. E., and Ledford, R. L. "Compensation of Dynamic Sting Effects in Hotshot Force Measurements." AEDC-TR-62-122 (AD277055), June 1962.

16. Ledford, R. L., Smotherman, W. E., and Kidd, C. T. "Recent Developments in Heat-Transfer-Rate, Pressure, and Force Measurements for Hotshot Tunnels." AEDC-TR-66-228 (AD645764), January 1967.

APPENDIXES

I. ILLUSTRATIONS
II. TABLES
III. GENERAL APPLICABILITY OF COMPENSATION TECHNIQUES TO DYNAMIC MEASUREMENT DEVICES

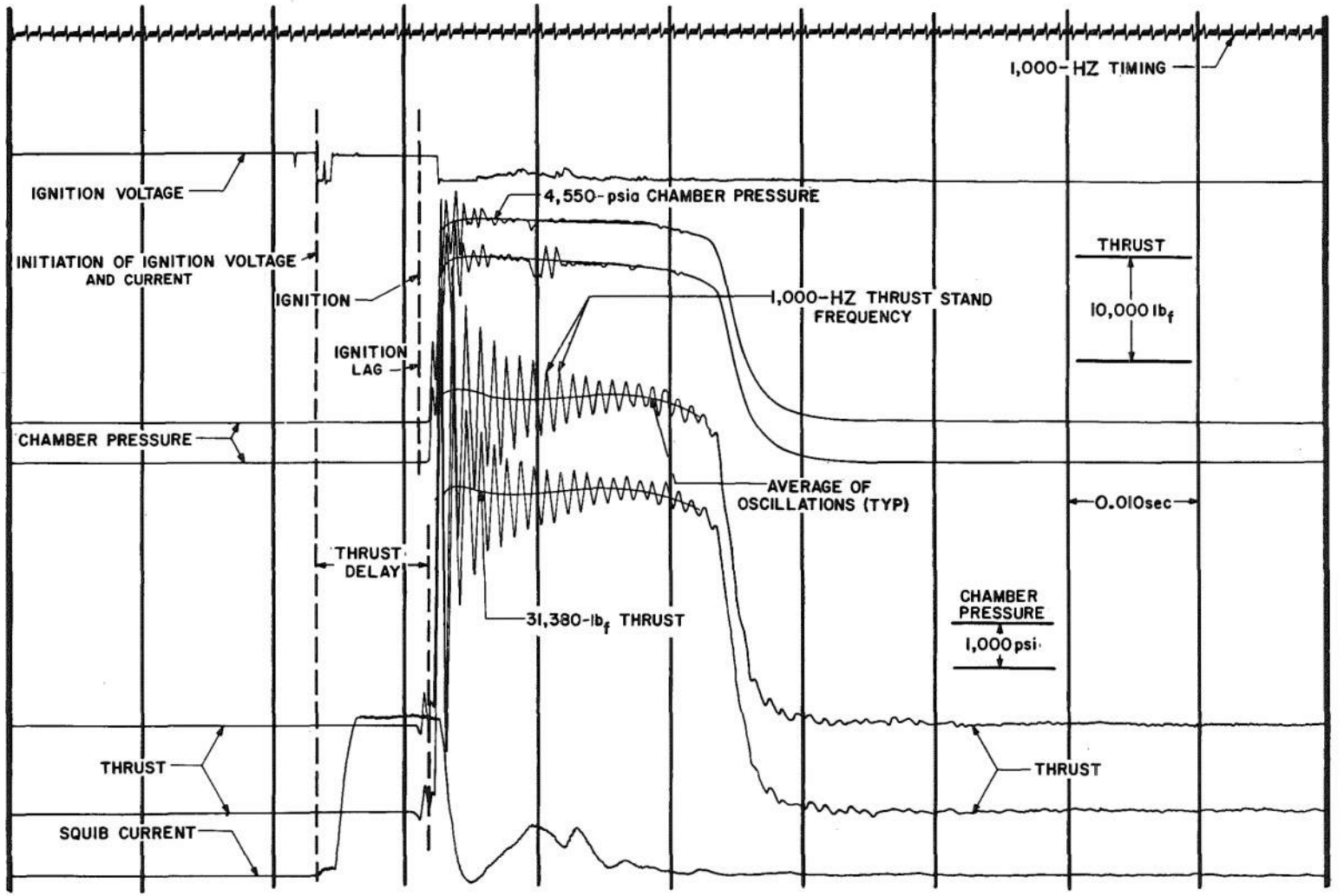

Fig. 1 Solid-Propellant Rocket Motor Test Data

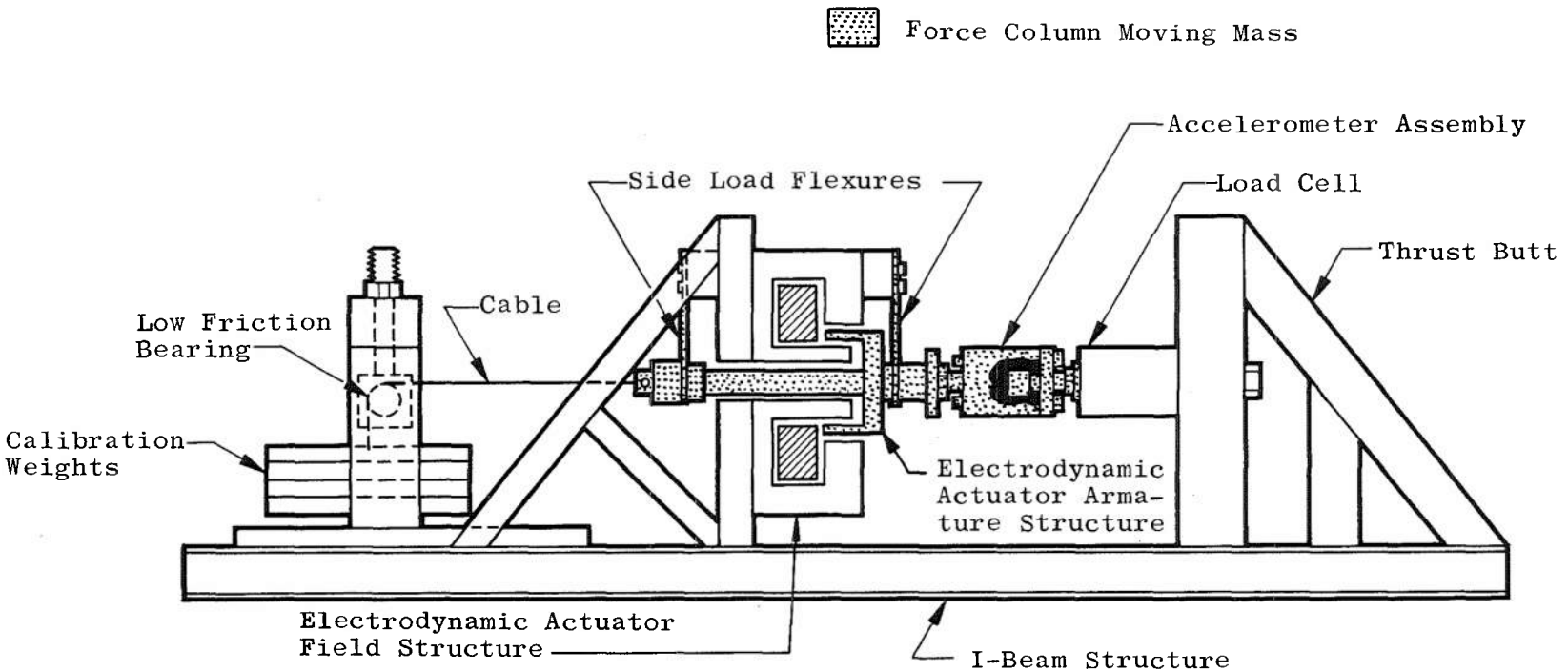

Fig. 2 Experimental Thrust Stand

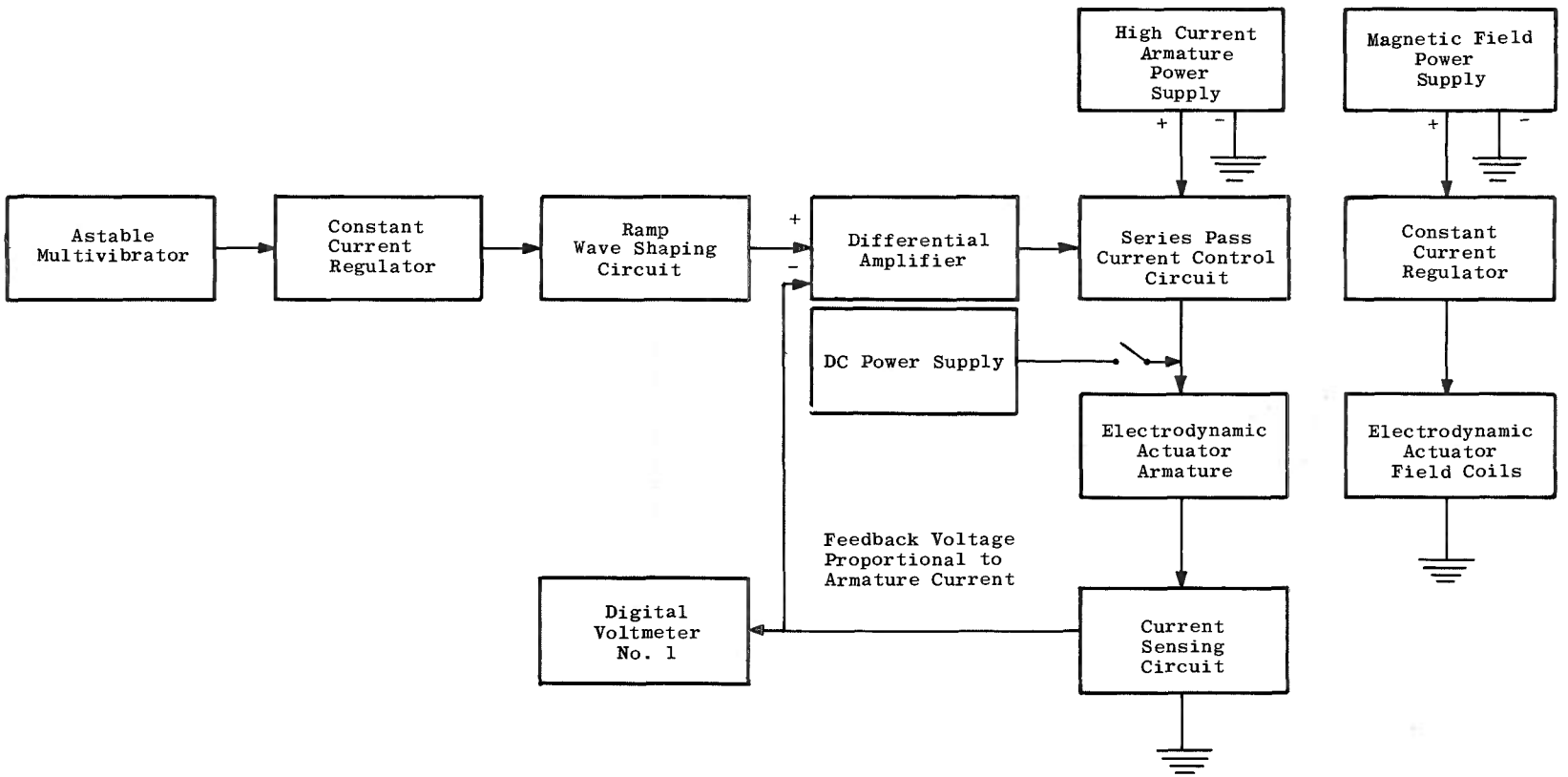

Fig. 3 Block Diagram of Current Function Generator and Electrodynamic Actuator

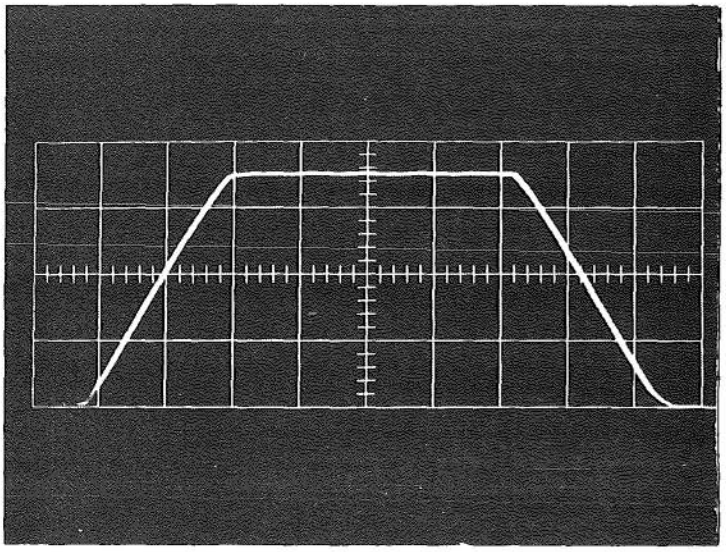

Horizontal Scale - 10 msec/cm
Vertical Scale - 9338.8 gm/cm,
20.57 lb/cm

a. Dynamic Force Calibrator Peak Force - 32,688 gm, 72 lb

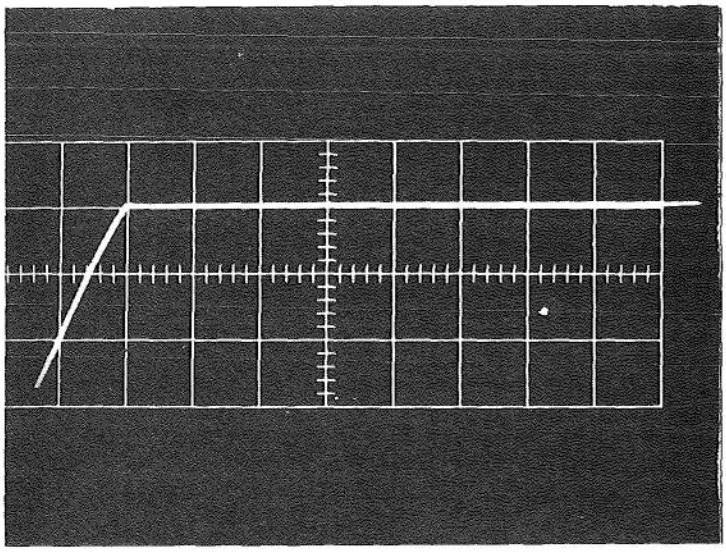

Horizontal Scale - 0.5 msec/cm
Vertical Scale - 4721.6 gm/cm,
10.4 lb/cm

b. Dynamic Force Calibrator Peak Force - 14,164.8 gm, 31.2 lb

Fig. 4 Typical Performance of the Current Function Generator for the Dynamic-Force Calibrator

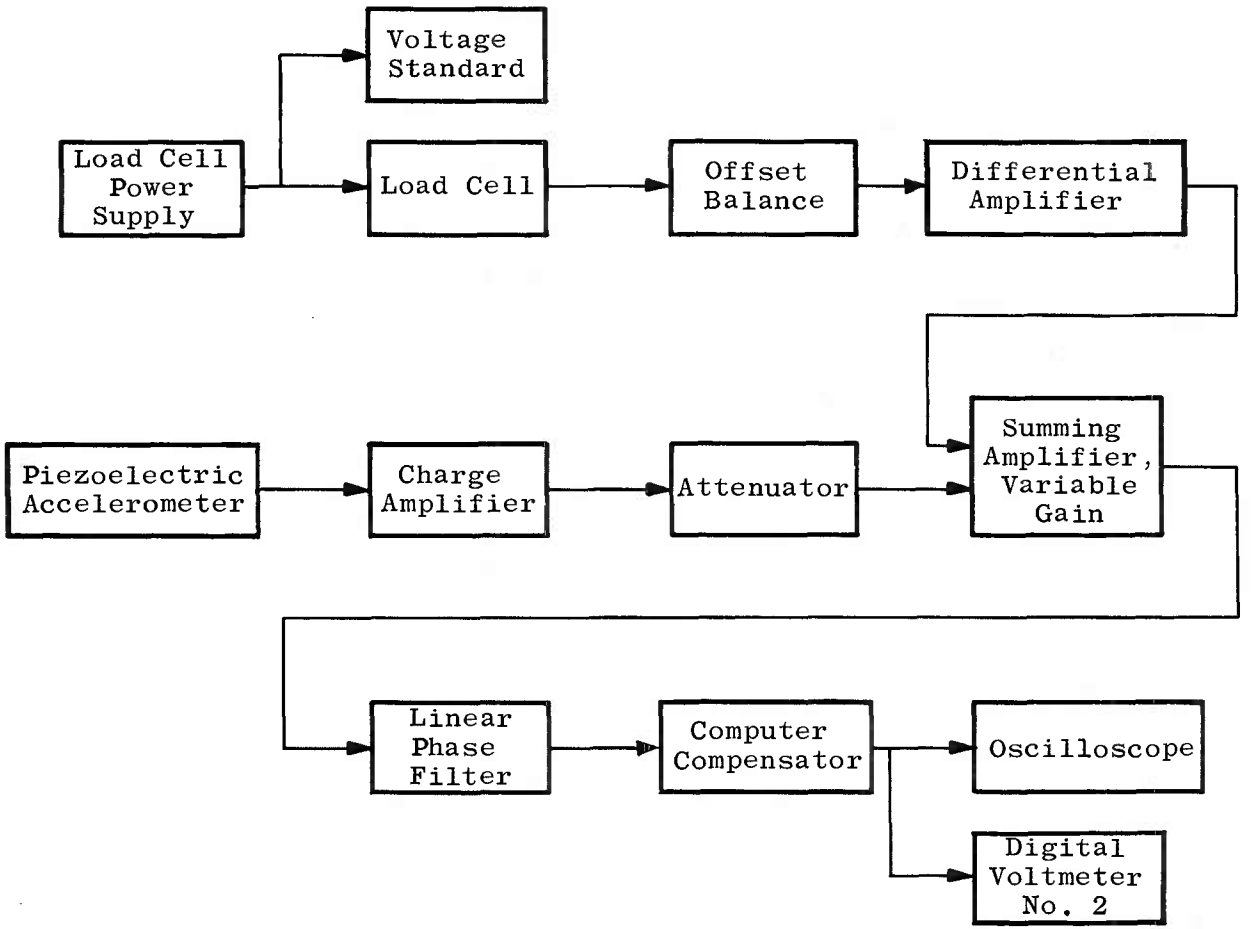

Fig. 5 Black Diagram of Hybrid System Transducers and Electronic Components

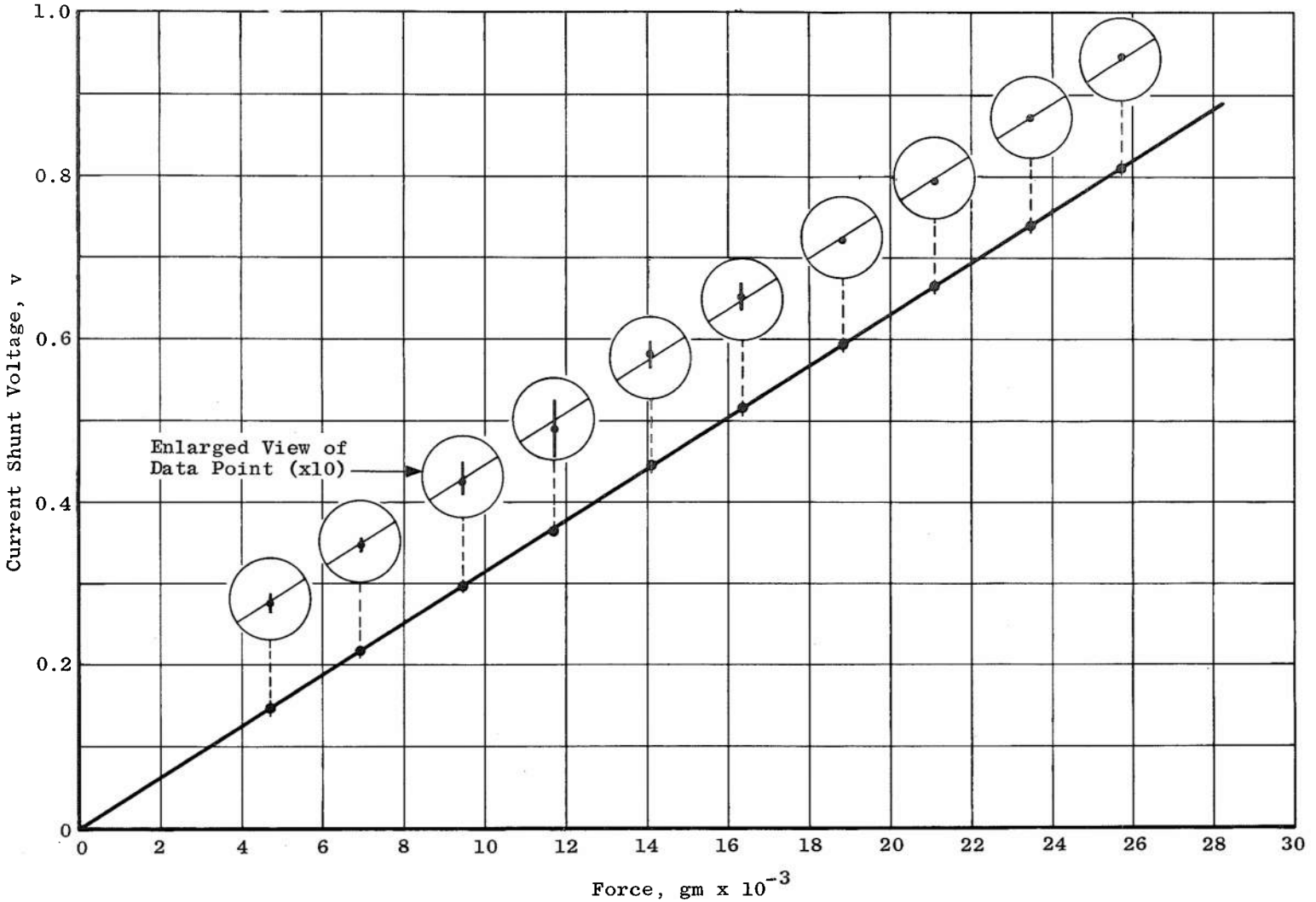

Fig. 6 Electrodynamic Actuator Static-Force Calibration Plot

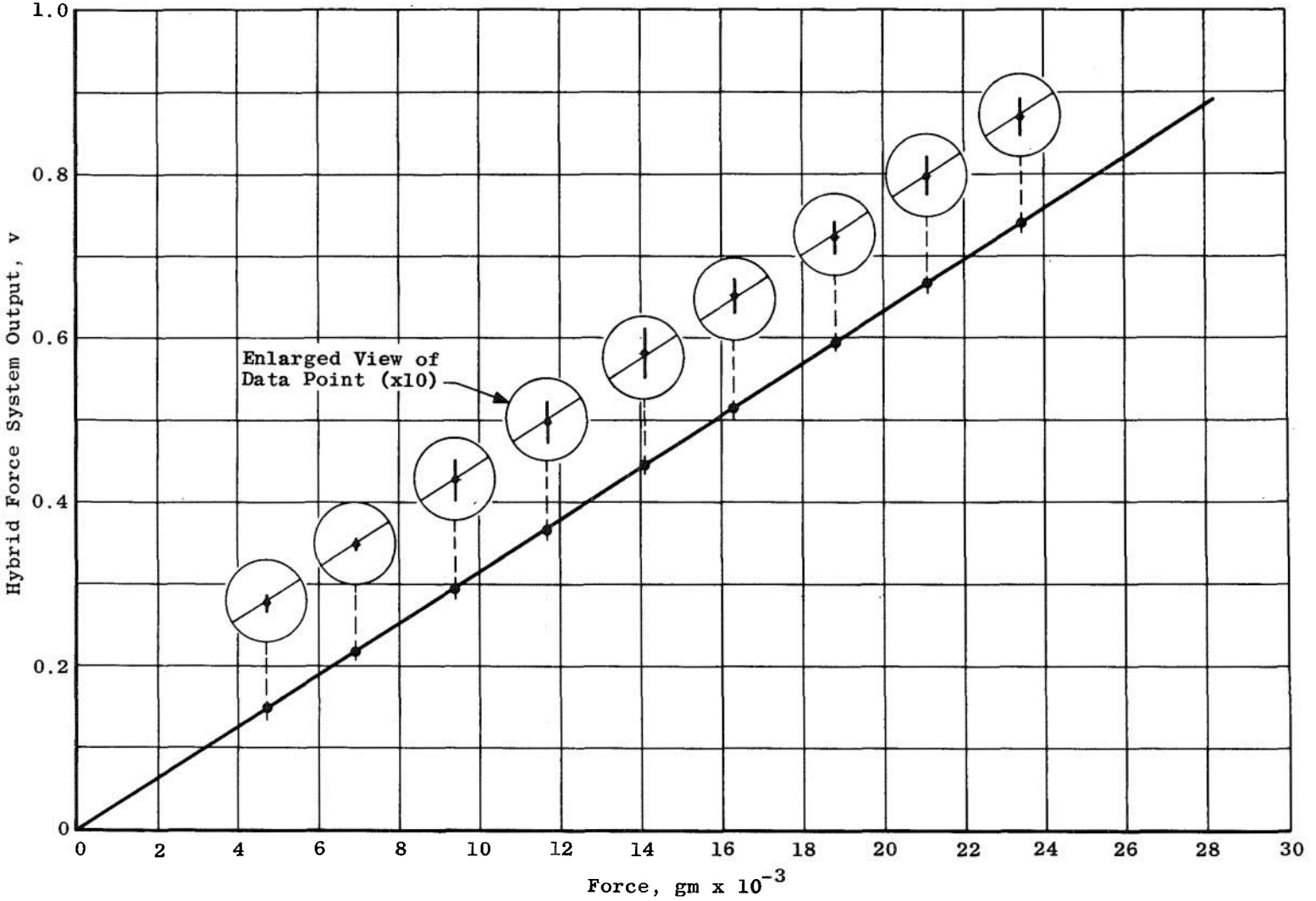

Fig. 7 Hybrid System Static-Force Calibration Plot

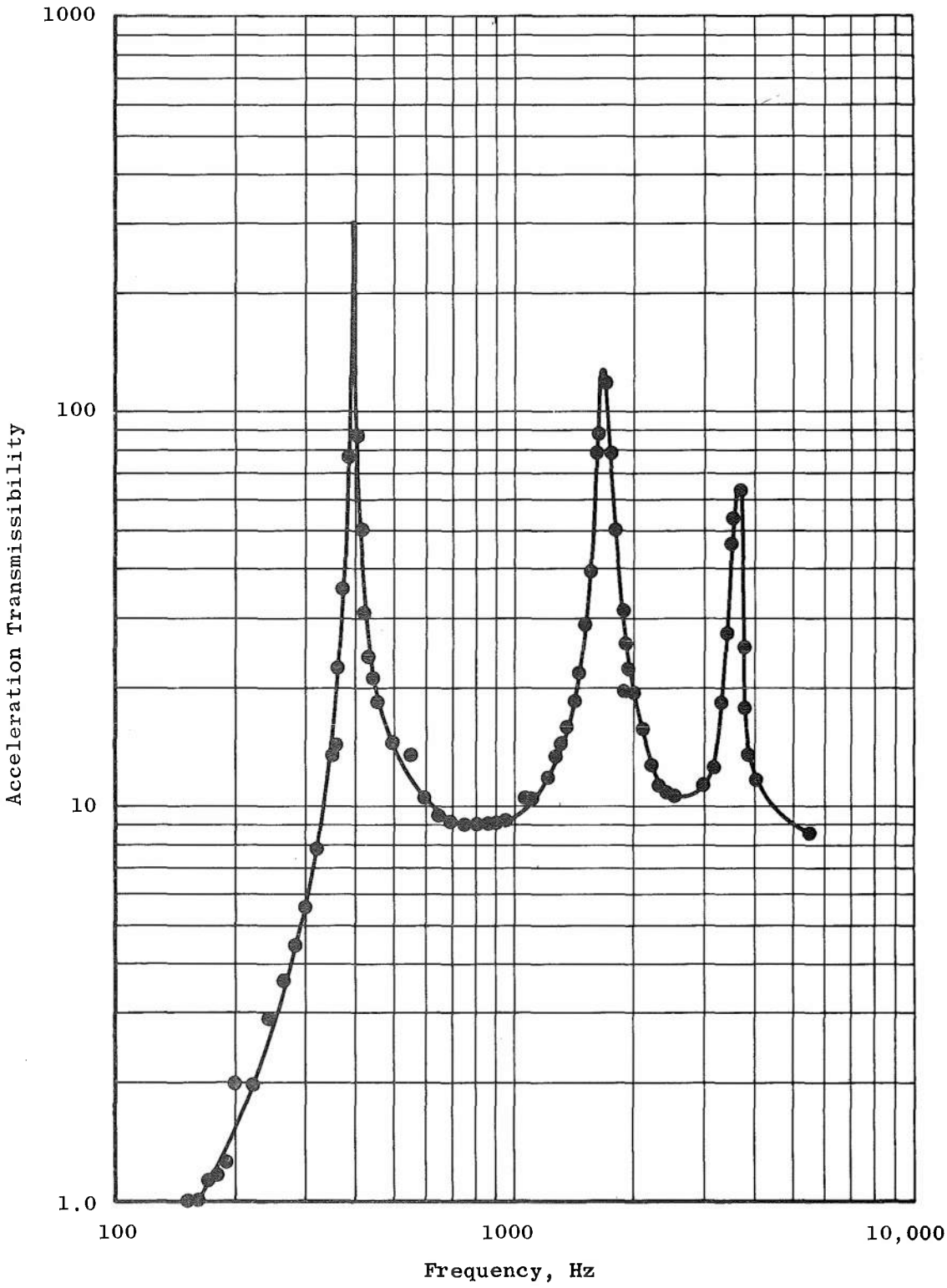

Fig. 8 Frequency Domain Characteristics - Acceleration Transmissibility

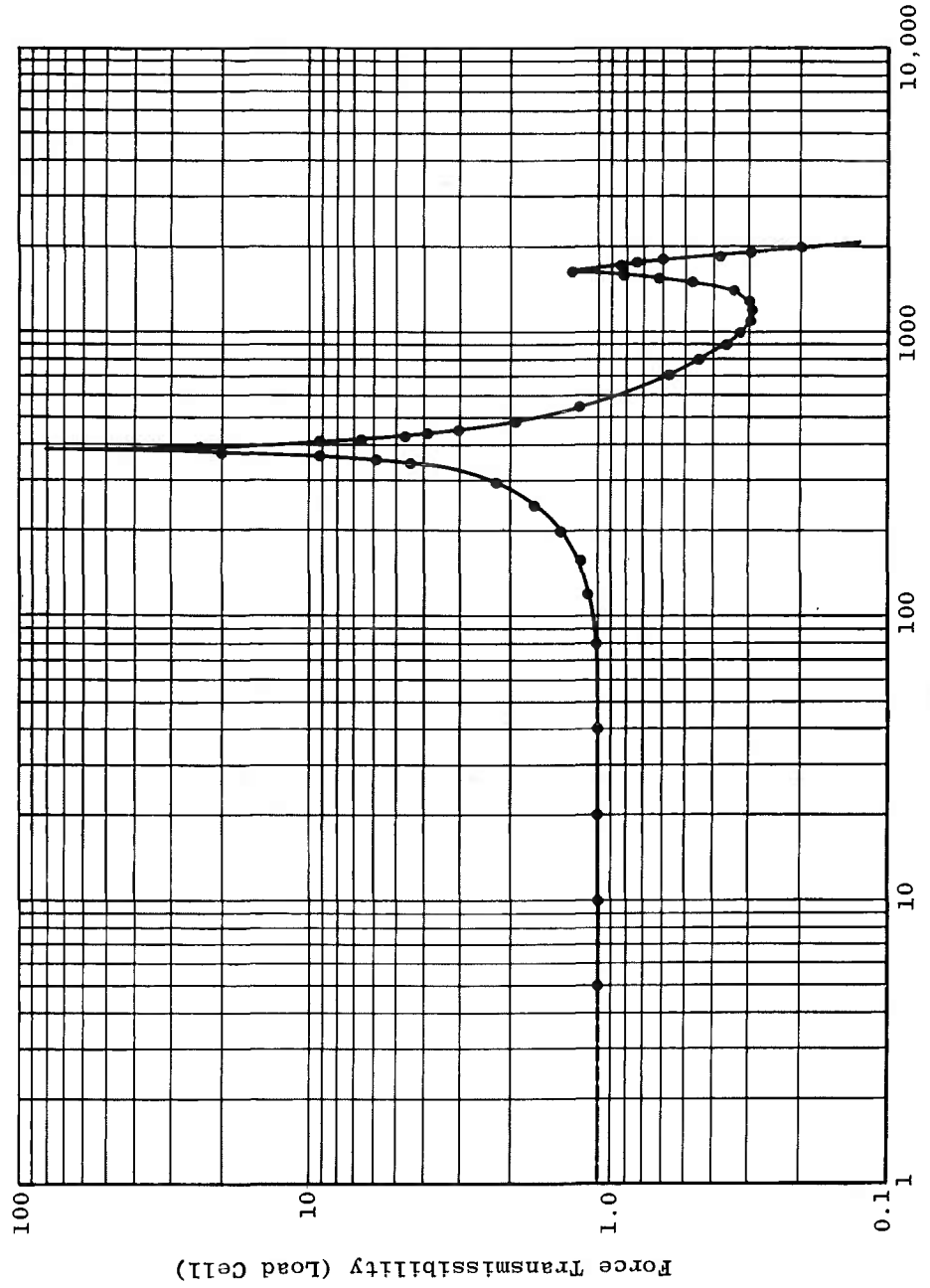

Fig. 9 Frequency Domain Characteristics - Load Cell Force Transmissibility

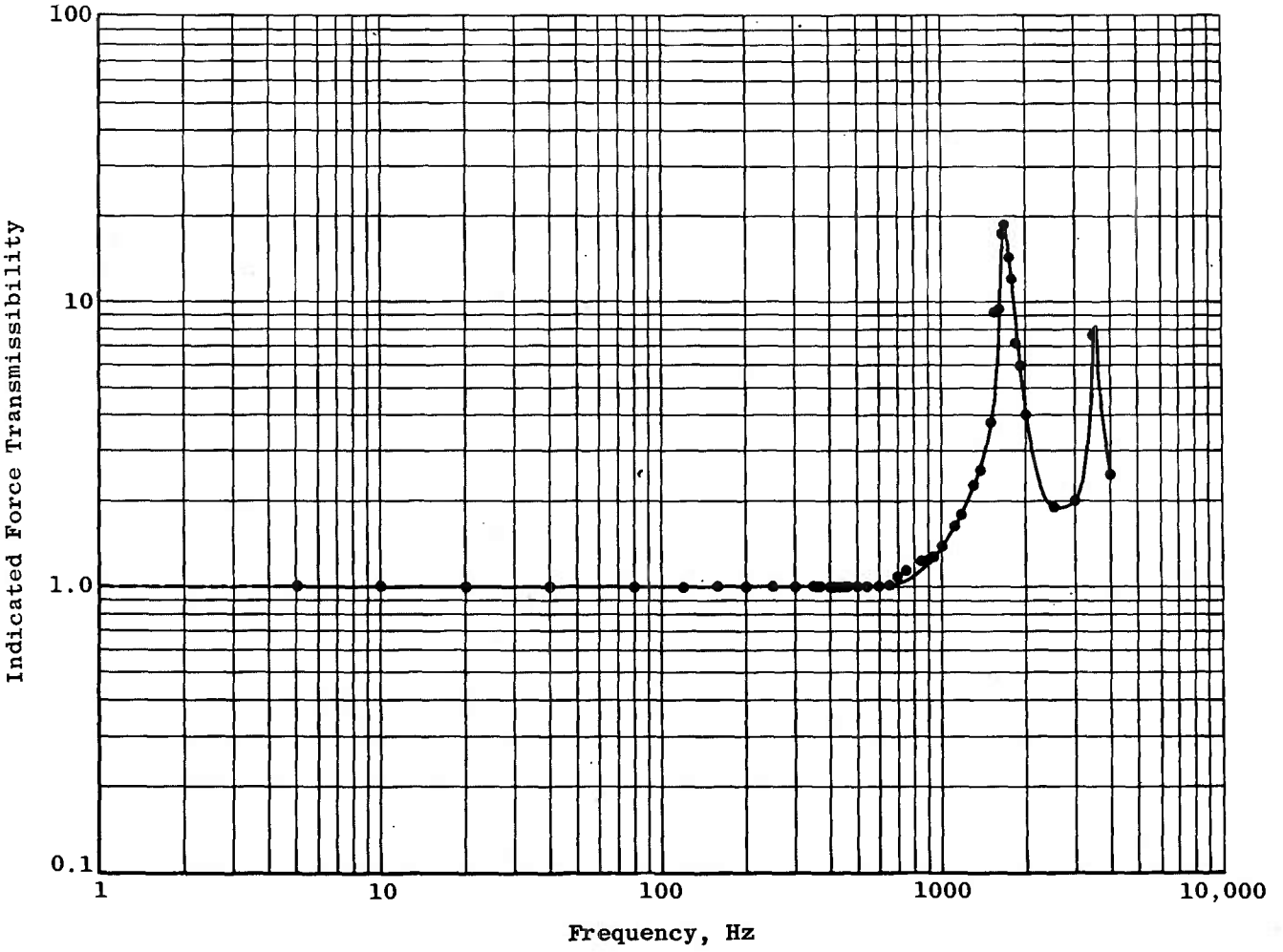

Fig. 10 Frequency Domain Characteristics - Reaction-Force Summation System Indicated Force Transmissibility

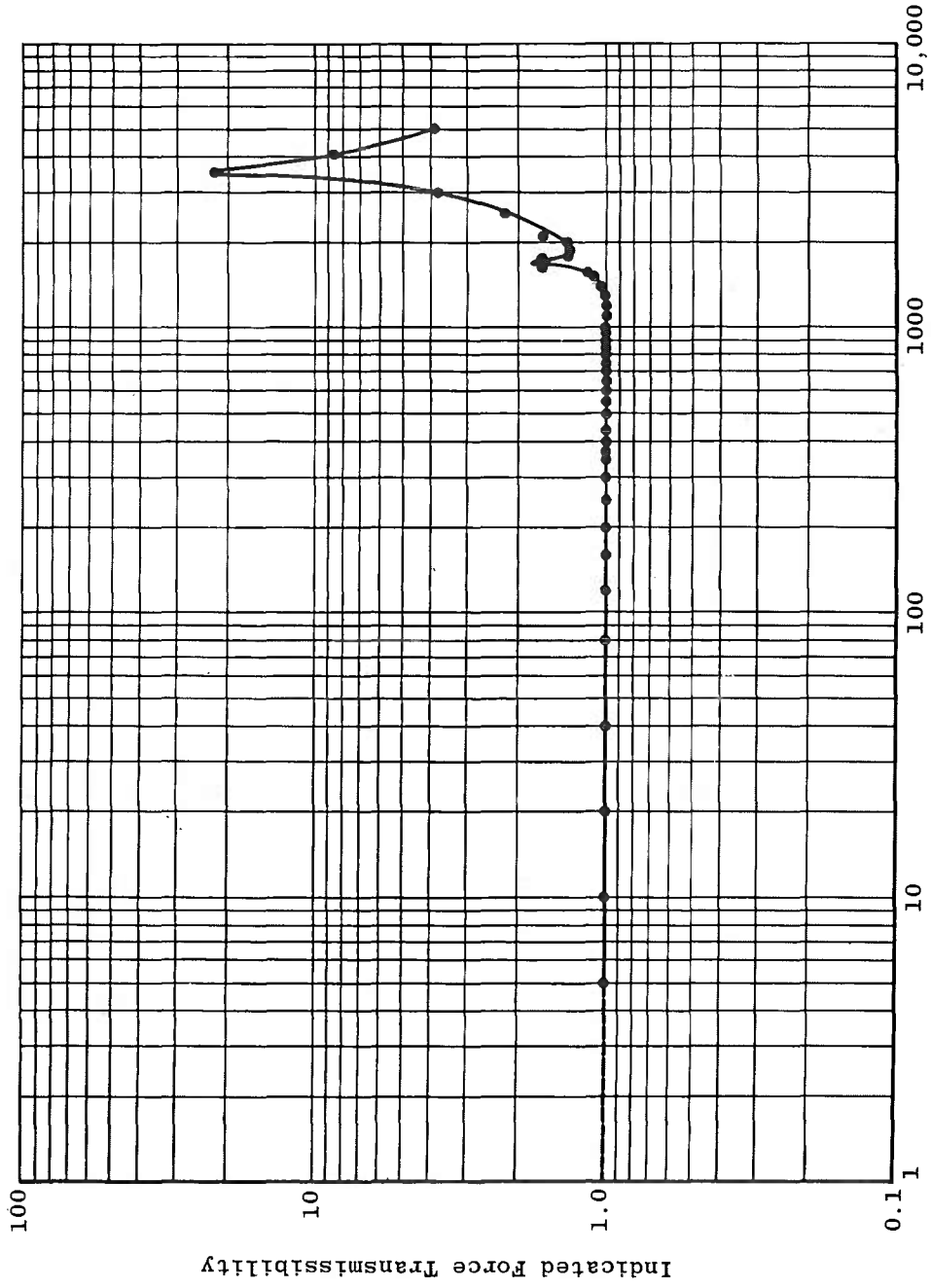

Fig. 11 Frequency Domain Characteristics - Hybrid System Indicated Force Transmissibility

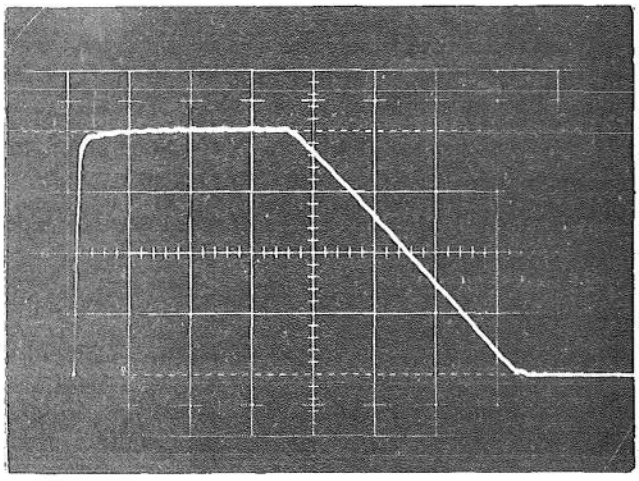

Horizontal Scale - 10 msec/cm
Vertical Scale - 6500 gm/cm,
14.32 lb/cm
Calibrator Peak Force -
26 kg, 57.26 lb

a. Dynamic-Force Calibrator Force-Time Function

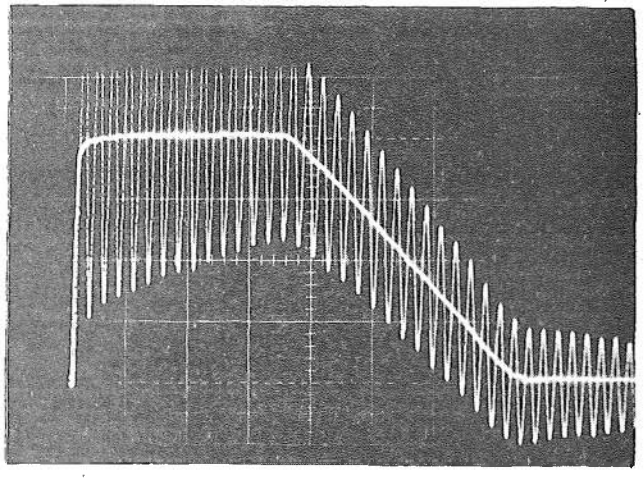

Horizontal Scale - 10 msec/cm
Vertical Scale - 6500 gm/cm,
14.32 lb/cm
Calibrator Peak Force -
26 kg, 57.26 lb

b. Load Cell Response Superimposed on the Calibrator Signal

Fig. 12 Time Domain Characteristics - Dynamic-Force Calibration Sequence

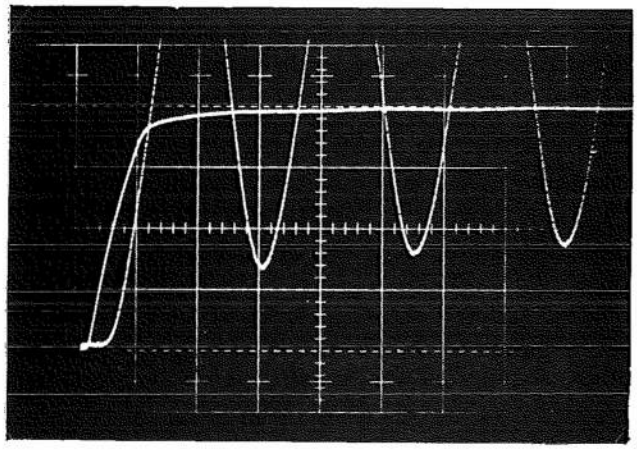

Horizontal Scale - 1 msec/cm
Vertical Scale - 6500 gm/cm, 14.32 lb/cm
Calibrator Peak Force - 26 kg, 57.26 lb

c. Load Cell Response Superimposed on the Calibrator Signal

Fig. 12 Continued

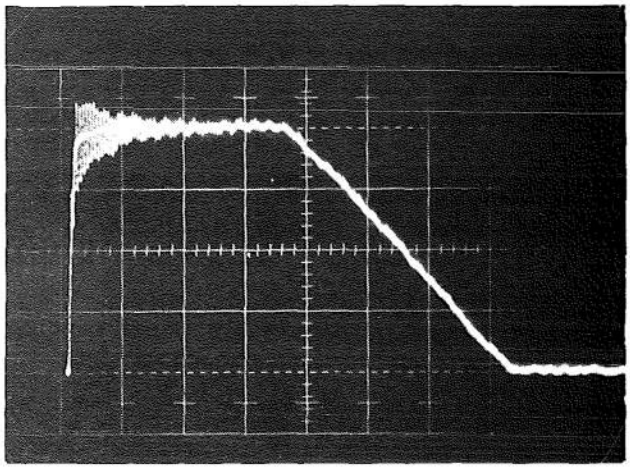

Horizontal Scale - 10 msec/cm
Vertical Scale - 6500 gm/cm,
14.32 lb/cm
Calibrator Peak Force -
26 kg, 57.26 lb

d. Reaction-Force Summation Signal Superimposed on the Calibrator Signal

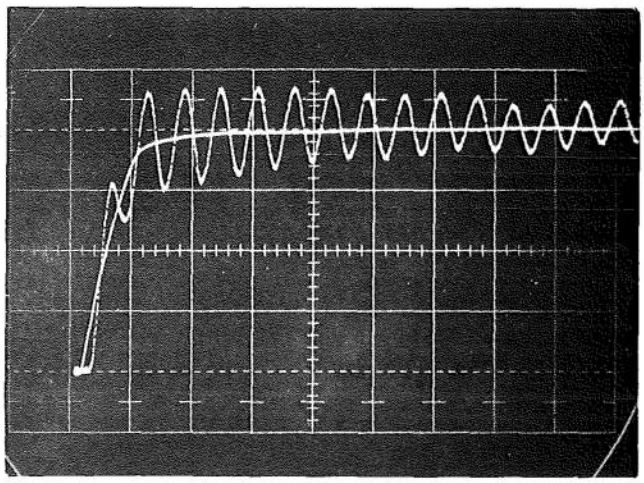

Horizontal Scale - 1 msec/cm
Vertical Scale - 6500 gm/cm,
14.32 lb/cm
Calibrator Peak Force -
26 kg, 57.26 lb

e. Expanded Time Scale Photograph of above

Fig. 12 Continued

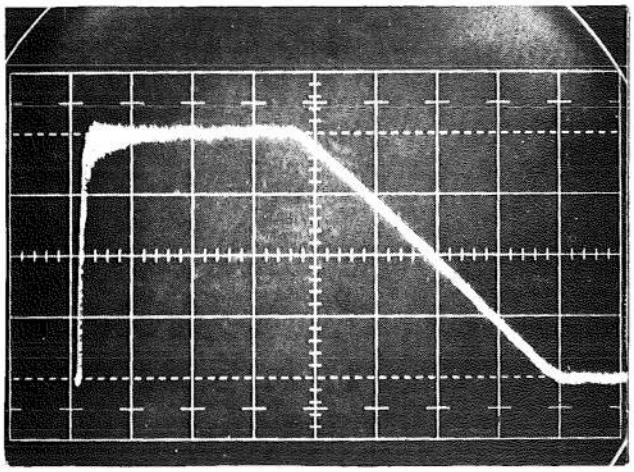

Horizontal Scale - 10 msec/cm
Vertical Scale - 6500 gm/cm
14.32 lb/cm
Calibrator Peak Force -
26 kg, 57.26 lb

f. Computer-Compensated Signal Superimposed on the Calibrator Signal

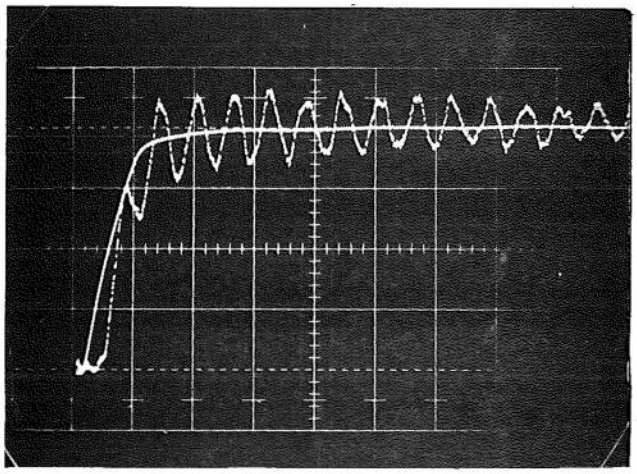

Horizontal Scale - 1 msec/cm
Vertical Scale - 6500 gm/cm
14.32 lb/cm
Calibrator Peak Force -
26 kg, 57.26 lb

g. Expanded Time Scale Photograph of above

Fig. 12 Continued

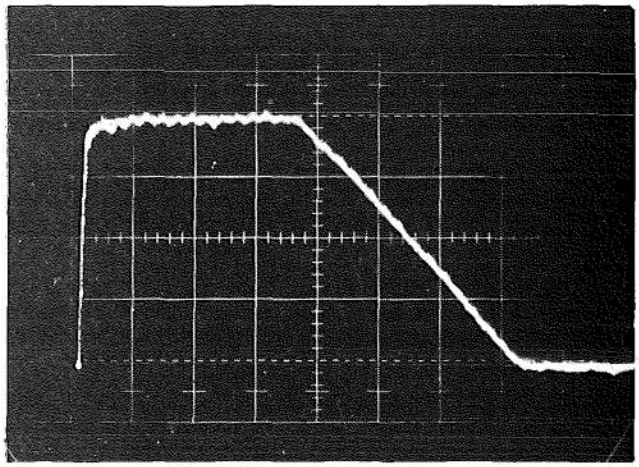

Horizontal Scale - 10 msec/cm
Vertical Scale - 6500 gm/cm,
14.32 lb/cm
Calibrator Peak Force -
26 kg, 57.26 lb

h. Hybrid System Signal Superimposed on the Calibrator Signal

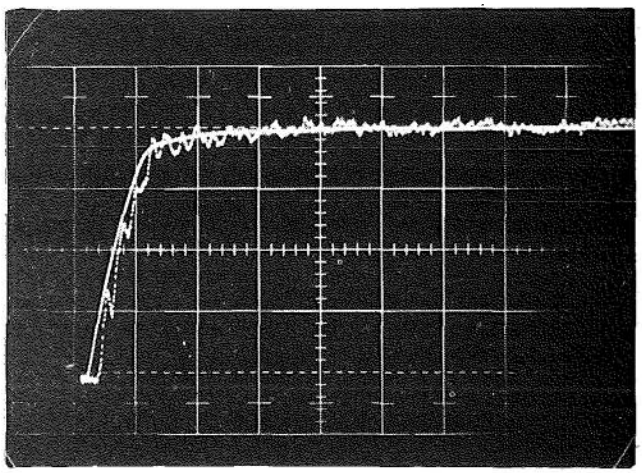

Horizontal Scale - 1 msec/cm
Vertical Scale - 6500 gm/cm,
14.32 lb/cm
Calibrator Peak Force -
26 kg, 57.26 lb

i. Expanded Time Scale Photograph of above

Fig. 12 Concluded

Horizontal Scale - 1 msec/cm
Vertical Scale - 6500 gm/cm, 14.32 lb/cm
Calibrator Peak Force - 22,230 gm, 48.97 lb

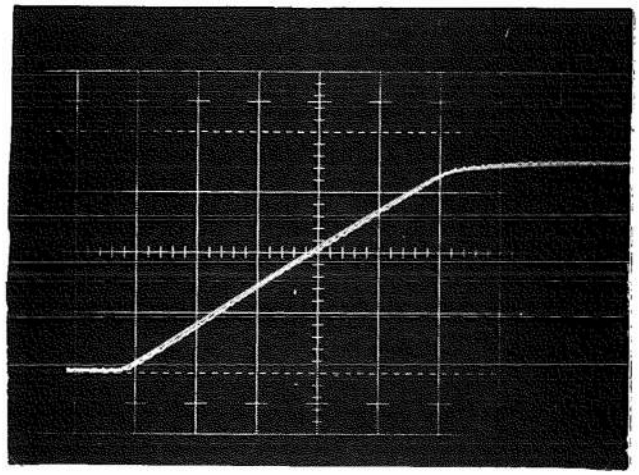

Hybrid System Signal Superimposed
on the Calibrator Signal

Fig. 13 Hybrid System Instantaneous Tracking Error Characteristics for a 5-msec Rise Time Force

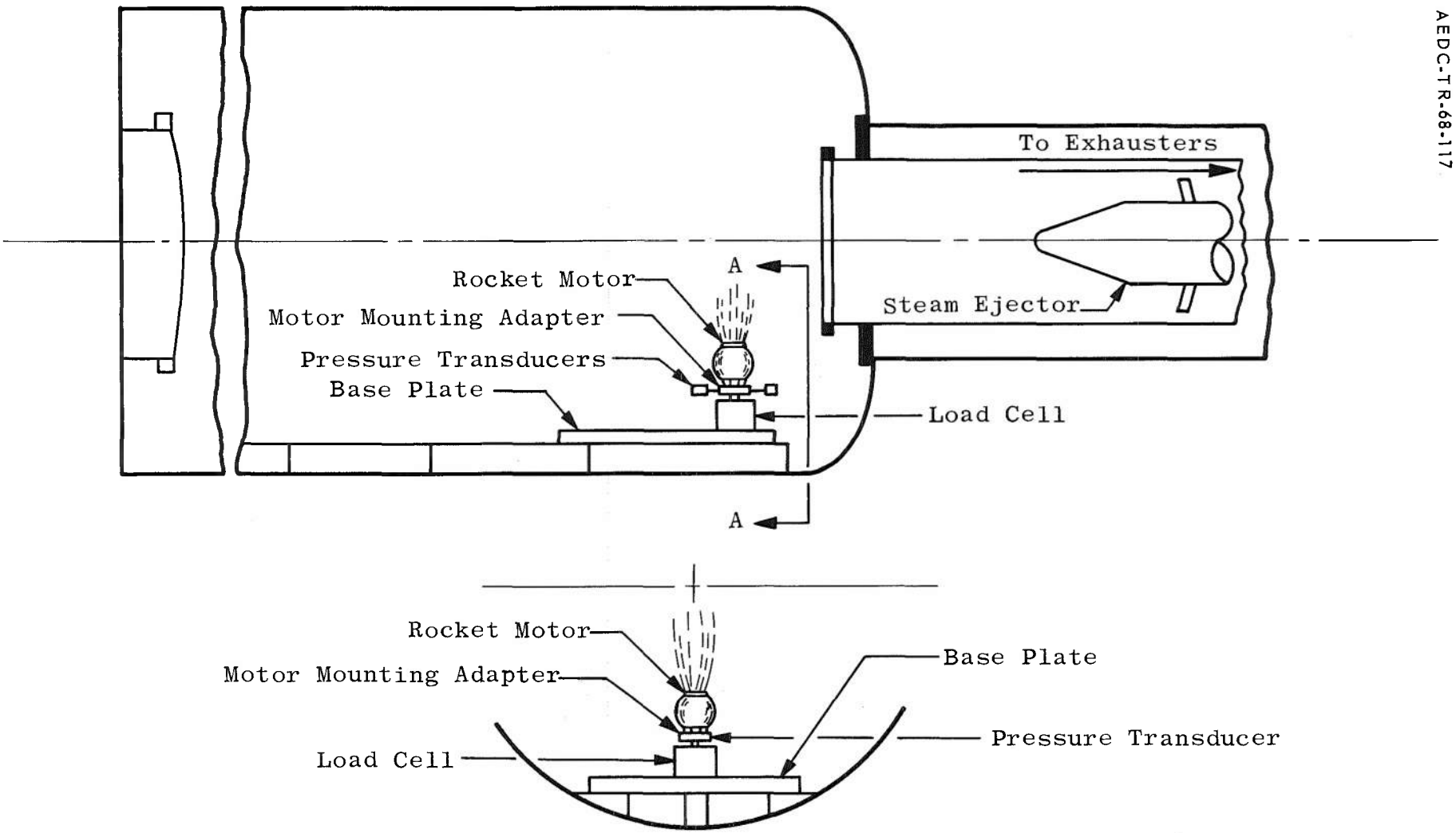

Fig. 14 Vertically Oriented Thrust Stand

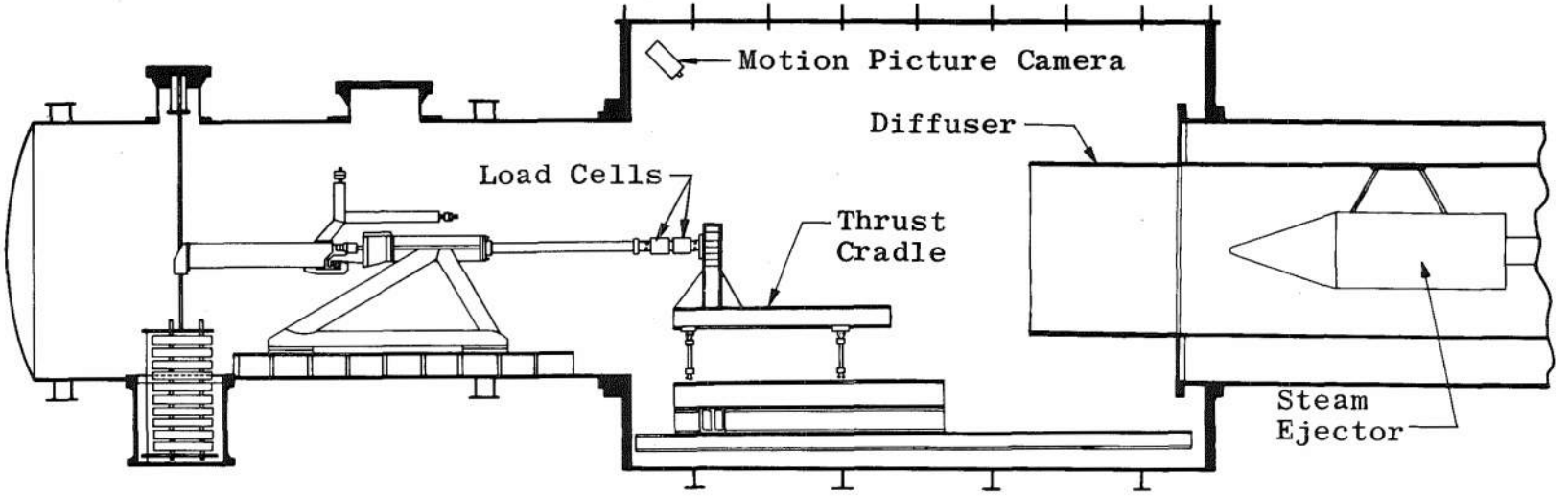

a. Conventional Thrust Stand

Fig. 15 Horizontally Oriented Thrust Stand

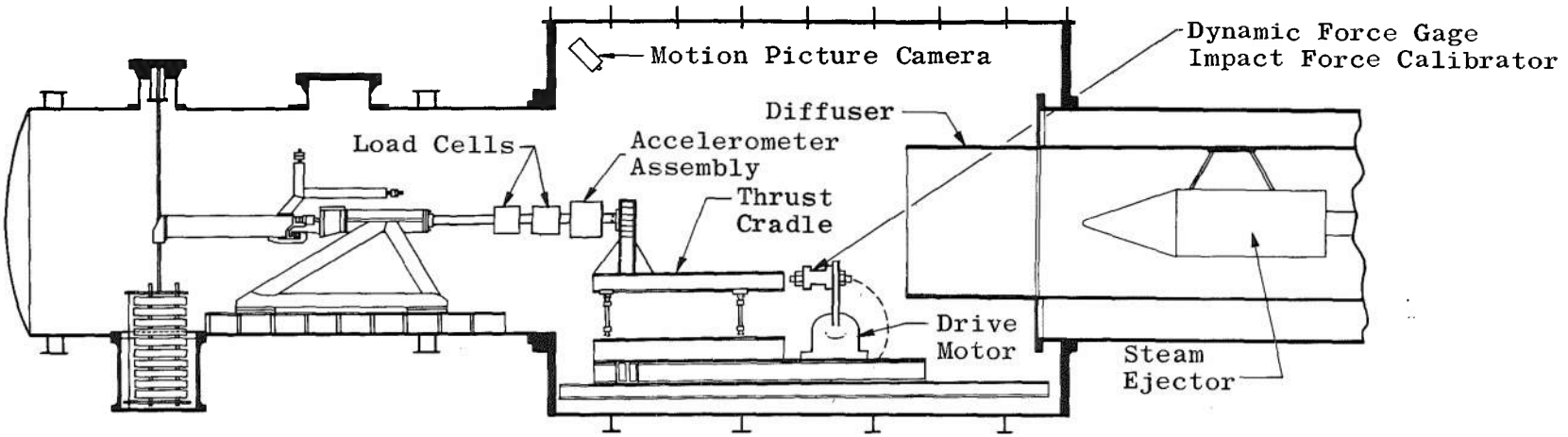

b. Proposed Modifications to Accomodate Dynamic-as Well as Static-Thrust Force Measurements.

Fig. 15 Concluded

TABLE I
STATISTICAL DATA - ELECTRODYNAMIC ACTUATOR
STATIC-FORCE CALIBRATION

Deadweight, gm	Shunt Voltage* (Arithmetic Average of Eight Readings Except Where Noted Otherwise), v	Standard Deviation, v x 10^3	95-percent Confidence Interval, v x 10^3
4,726	0.146_2	0.8	1.3
6,986	0.218_7	0.5	0.8
9,449	0.297_0	1.2	2.0
11,709	0.367_0	2.1	3.5
14,128	0.448_2	1.0	1.7
16,388	0.518_9	1.0	1.7
18,853	0.592		
21,113	0.663		
23,456	0.739	Single Calibration Readings Taken at These Points	
25,716	0.811		
28,128	0.885		

*Fourth significant digit results from the arithmetic averaging procedure.

TABLE II
STATISTICAL DATA - HYBRID SYSTEM STATIC-FORCE CALIBRATION

Deadweight, gm	Hybrid System Output Signal* (Arithmetic Average of Eight Readings), v	Standard Deviation, v x 10^3	95-percent Confidence Interval, v x 10^3
4,726	0.146_0	0.6	1.0
6,986	0.218_8	0.4	0.6
9,449	0.296_4	1.6	2.7
11,709	0.367_0	1.7	2.8
14,128	0.447_0	1.8	3.0
16,388	0.518_4	1.2	2.0
18,853	0.592_1	1.2	2.0
21,113	0.665_4	1.2	2.0
23,456	0.736_3	1.4	2.3
28,128	0.885_0	1.6	2.7

*Fourth significant digit results from the arithmetic averaging procedure.

APPENDIX III
GENERAL APPLICABILITY OF COMPENSATION TECHNIQUES TO DYNAMIC MEASUREMENT DEVICES

Dynamic compensation techniques are generally applicable for many dynamic measurement systems, in addition to the force measurement system discussed in the present report. This appendix contains a brief summary of the basic considerations involved in applying the reaction-force summation and analog computer compensation techniques to first-, second-, and higher-order linear measurement systems. Several applications of dynamic compensation techniques at the AEDC are discussed.

DYNAMIC MEASUREMENT SYSTEM CHARACTERISTICS REQUIRED TO EFFECT DISTORTIONLESS MEASUREMENTS

The forcing function input to any linear, time-invariant physical system (such as mechanical or electrical) can be related analytically to the system output response by the system transfer function:

$$F(j\omega)\, G(j\omega) = X(j\omega) \tag{III-1}$$

where $j\omega$ is the Fourier transform variable, $F(j\omega)$ is the Fourier transformed forcing function, $G(j\omega)$ is the system transfer function, and $X(j\omega)$ is the Fourier transformed system output response. Specifically, $G(j\omega)$ may be the transfer function of a certain dynamic measurement system (such as force, pressure, or temperature) used to measure $F(j\omega)$. In this case, it is obvious that $G(j\omega)$ should be a form such that distortionless measurements of $F(j\omega)$ are possible. If the system transfer function is of the form

$$G(j\omega) = h = \text{constant scale factor} \tag{III-2}$$

then $X(j\omega)$ is just a scaled replica of $F(j\omega)$, and distortionless measurements of $F(j\omega)$ are possible. Equation (III-2) describes a dynamic measurement system with a transfer function that is frequency independent. This condition is not always possible to approximate. If the measurement system is frequency dependent, then distortionless but time-delayed measurements are possible if the system transfer function is of the form (Ref. 10):

$$G(j\omega) = h \exp(-j\omega t_d) \tag{III-3}$$

where h is a constant scale factor, t_d is a constant phase delay, and exp is the base of the natural logarithm. It is important to realize that although a basic measurement system transfer function, $G_1(j\omega)$, may not conform

to the conditions dictated by Eq. (III-3), dynamic compensation components with a transfer function $G_2(j\omega)$ may be included in the measurement system electronic circuitry so that the overall system transfer function does conform to Eq. (III-3):

$$G_1(j\omega)\, G_2(j\omega) = G(j\omega) = h \exp(-j\omega t_d) \qquad \text{(III-4)}$$

Equation (III-4) is a basic mathematical description of the use of a compensating transfer function, $G_2(j\omega)$, to reconstruct forcing function information that has been distorted by the basic measurement system transfer function, $G_1(j\omega)$ (Refs. 5 and 6). The transfer function, $G_2(j\omega)$, can be generated with operational amplifier circuitry, and this procedure is sometimes termed "the analog computer compensation technique."

In practical applications (using operational amplifier circuitry), $G_2(j\omega)$ may be programmed to compensate for the transient response distortions caused by two or possibly three natural frequencies of the system. A separate stage of computer circuitry is required for each natural frequency to be compensated. Computer compensator circuitry can compensate for natural frequencies from several to several hundred thousand Hertz (Ref. 5).

Two types of analog computer compensation circuits have been developed to a high degree by personnel of the Rocket Test Facility at the AEDC (Refs. 11 and 12). These circuits were used to compensate for natural-frequency distortions in rocket thrust stand data.

Dynamic-Force Measurement Systems

Conventional force measurement systems such as rocket thrust stands and pressure measurement systems are often incapable of performing distortionless dynamic measurements because of the inadequate dynamic response characteristics of the basic transducer used. However, auxiliary motion-sensing transducers can often be utilized in a somewhat unconventional manner in conjunction with the basic transducer to yield distortionless dynamic- (as well as static) force measurements. For the sake of illustration, assume that the equation of motion of a dynamic-force measurement system is given by[1]

$$M\ddot{x}(t) + K x(t) = F(t) \qquad \text{(III-5)}$$

[1]This is a valid assumption for any linear, single-degree-of-freedom, time-invariant, undamped system. Specifically, Eq. (III-5) adequately describes most high quality pressure transducers which are not significantly damped by the fluid whose pressure is being measured. Equation (III-5)

where M is the moving mass and K is the spring constant of the measurement system, x(t) is the displacement of M, $\ddot{x}(t)$ is the acceleration of M, and F(t) is the dynamic force to be measured. In the conventional force measurement system, only the Kx(t) term of Eq. (III-5) is measured (by the basic transducer) and recorded as the analog representation of F(t), and the $M\ddot{x}(t)$ is neglected. Unless Kx(t) is much greater than $M\ddot{x}(t)$, significant distortion of the measurement signal is to be expected during rapid changes in the input force. The design objective of the rocket thrust stand described in Ref. 2 was to provide a predominantly single-degree-of-freedom thruster-thrust stand structure with stiffness so great that the Kx(t) term of Eq. (III-5) would be much greater than the $M\ddot{x}(t)$ term for any expected F(t). This type of thrust measurement system would conform to the distortionless measurement criterion set forth in Eq. (III-2), and the scale factor, h, would be equal to 1/K.

When the moving mass, M, is large, it is impractical, if not impossible, to provide a Kx term much larger than the $M\ddot{x}$ term. In this case, a straightforward consideration of Newton's third law of motion (expressed by Eq. (III-5) for this particular discussion) leads to the measurement and summation of both reaction-force terms, Kx and $M\ddot{x}$, as the analog representation of F(t). This is the essence of the "reaction-force summation" or "acceleration compensation" dynamic-force measurement technique, and this technique is quite easily applied for systems described by Eq. (III-5).

A quite valuable asset of the reaction-force summation technique is its insensitivity to forces introduced through the base (as opposed to the active end) of the Kx transducer (Refs. 4 and 6). For a thrust measurement system this means that forces introduced through the base of the load cell because of thrust butt motions will not distort the thrust measurement information.

Multiple-degree-of-Freedom Dynamic-Force Measurement Systems

The computer compensation technique can theoretically be used to compensate for any number of degrees of freedom of a force measurement system. However, experience has shown that compensation for two or possibly three degrees of freedom is a practical limit.

---

accurately describes certain rocket thrust force measurement systems such as the type shown in Fig. 14 where the predominant damping mechanism is caused by structural deformations of the basic force measurement transducer (load cell). Load cell deformation damping for virtually any rocket thrust stand load cell would contribute a negligible damping force to Eq. (III-5). This equation obviously does not accurately describe multiple-degree-of-freedom thrust stands such as those shown in Figs. 2 and 15.

The reaction-force summation technique is insensitive to forces introduced through the base of the Kx(t) transducer, regardless of the degrees of freedom of the base structure, but can compensate for only one degree of freedom of the structure attached to the active end of the Kx(t) transducer.

The "hybrid" combination of the unique capabilities of the reaction-force summation and computer compensation techniques has previously been proposed in Ref. 6 to compensate for multiple-degree-of-freedom response of rocket thrust stands. This hybrid system has been evaluated in the present report and has been shown to yield accurate and precise dynamic-force measurements for a three-degree-of-freedom experimental thrust stand.

COMPENSATION FOR LINEAR FIRST-ORDER SYSTEMS

The linear first-order system differential equation is:

$$\tau_1 \dot{X}(t) + X(t) = F(t) \qquad \text{(III-6)}$$

where τ_1 is the system time constant, X(t) is the response variable, $\dot{X}(t)$ is the first time derivative of X(t), and F(t) is the forcing function. Using Laplace transform terminology, Eq. (III-6) can be put into the form

$$X(s) = F(s)\, G_1(s) = F(s) \left(\frac{1}{\tau_1 s + 1}\right) \qquad \text{(III-7)}$$

where s is the Laplace transform variable. In many first-order measurement systems, such as a thermocouple or resistance-type temperature measurement system, the time constant τ_1 is undesirably large so that the response variable cannot accurately follow dynamic changes of the forcing function; i.e., the system transfer function does not conform to the requirement set forth in Eq. (III-2). To improve the dynamic response characteristics, a stage of computer compensation circuitry can be used in conjunction with the basic measurement system to yield an overall transfer function that conforms with the criterion set forth in Eqs. (III-3) and (III-4) and that has a much smaller time constant than the uncompensated system. For example, a thermocouple temperature measurement system produces an output voltage $e_o(t)$ for a static temperature, T. If T changes rapidly compared to the time constant, τ_1, of the thermocouple, then the equation describing the situation is

$$\tau_1 \dot{e}(t) + e(t) = e_o(t) \qquad \text{(III-8)}$$

where $e_o(t)$ is the instantaneous voltage that would be produced by the thermocouple at an instantaneous value of temperature, T, if the thermocouple had a zero time constant. The transfer function of the thermocouple

is $G_1(s)$ in Eq. (III-7). The computer compensator circuitry shown in Fig. III-1 produces the following transfer function:

$$\frac{e_o(s)}{e_{in}(s)} = G_2(s) = \frac{(\tau_1 s + 1)}{(\tau_2 s + 1)} \qquad \text{(III-9)}$$

where τ_1 is determined by the value of R, C_1, and C_2 and τ_2 is determined by the value of R and C_2. The resistance, R, and the capacitance, C_2, can be independently chosen so that $\tau_2 << \tau_1$ and improved dynamic response will result since the overall measurement system time constant will be reduced. This can be seen by forming the product $G_1(S)\ G_2(S)$:

$$G(s) = G_1(s)\, G_2(s) = \left(\frac{1}{\tau_1 s + 1}\right) \left(\frac{\tau_1 s + 1}{\tau_2 s + 1}\right) = \left(\frac{1}{\tau_2 s + 1}\right) \qquad \text{(III-10)}$$

It can be seen from Eq. (III-10) that the thermocouple pole is "cancelled" by the compensator zero. By setting $x = j\omega$, the overall transfer function of Eq. (III-10) can be seen to approximate the requirement for a distortionless measurement system transfer function set forth in Eq. (III-4):

$$G(s) = G_1(s)\, G_2(s) = \left(\frac{1}{\tau_2}\right) \left[\frac{1}{\left(\frac{1}{\tau_2^2} - \omega^2\right)^{1/2}}\right] \exp(-j\omega\tau_2) \qquad \text{(III-11)}$$

The approximation is good for that range of frequencies for which $\omega < \frac{1}{\tau_2}$.

Compensation techniques have been used in the past to decrease the overall time lag of thermocouple and resistance-type thermometers by three orders of magnitude (Ref. 13). The amount of decrease of the time lag is limited by the signal-to-noise characteristics of the basic transducer signal.

A description of a temperature measurement compensation system was given here as an example of compensation of first-order dynamic measurement systems, but it should be clear that the circuitry, shown in Fig. 16, could be used to compensate any first-order system with an electrical output signal. For example, compensation circuitry is routinely used to enhance the dynamic response characteristics of anemometers (Ref. 14).

COMPENSATION OF PRESSURE TRANSDUCER DATA

A high quality dynamic pressure transducer will exhibit predominantly linear, second-order, dynamic response characteristics so that its equation of motion is

$$A\, P(t) = F(t) = M\ddot{x}(t) + B\dot{x}(t) + Kx(t) \qquad \text{(III-12)}$$

where P(t) is the pressure to be measured; A is the area and M is the mass of the pressure-sensing diaphragm; B is the damping coefficient; K is the spring constant of the diaphragm spring restraint element; and x, $\dot{x}$, and $\ddot{x}$ are the displacement, velocity, and acceleration of the diaphragm, respectively.

In some cases, the damping force, $B\dot{x}$, is small and can be neglected. Equation (III-12) then becomes:

$$AP(t) = F(t) = M\ddot{x}(t) + Kx(t) \qquad \text{(III-13)}$$

and the reaction-force summation technique can be applied. The design and fabrication technology required to produce small but reliable diaphragm-mounted accelerometers has been developed by the Hypervelocity Instrumentation Section, von Kármán Gas Dynamics Facility (VKF), at the AEDC and these acceleration-compensated pressure transducers have been used in the VKF hotshot wind tunnels.

Computer compensation techniques can be used (independently of the reaction-force summation technique) to compensate for the natural-frequency distortion of pressure transducer information. The transfer function of a pressure transducer described by Eq. (III-12) is

$$G_1(s) = \left(\frac{\omega_0^2}{K}\right)\left(\frac{1}{s^2 + 2\zeta_0\omega_0 s + \omega_0^2}\right) \qquad \text{(III-14)}$$

where ω_0 is the natural radian frequency and ζ_0 is the damping ratio of the pressure transducer and fluid medium. A single stage of approximate differentiator-type computer compensation circuitry could be programmed to produce the following transfer function (Refs. 5 and 6):

$$G_2(s) = \frac{H(s^2 + 2\zeta_0\omega_0 s + \omega_0^2)}{(s + 12\omega_0)^2} \qquad \text{(III-15)}$$

where H is a constant. The tandem connection of the pressure transducer and computer compensator yields the following transfer function:

$$G_1(s)\,G_2(s) = G(s) = H\left[\frac{\omega_0^2}{K}\right]\left[\frac{1}{(s + 12\omega_0)^2}\right] \qquad \text{(III-16)}$$

and it can be seen that the compensator zeroes have "cancelled" the transducer poles. Equation (III-16) can be shown to approximate the frequency-dependent but distortionless transfer function set forth in Eq. (III-4) by setting $s = j\omega$ and writing Eq. (III-16) in the following form:

$$G_1(j\omega)\,G_2(j\omega) = G(j\omega) = \left\{\frac{H\omega_0^2}{K}\right\}\left\{\frac{\exp\left[-j\omega\left(\frac{24\omega_0}{144\omega_0^2 - \omega^2}\right)\right]}{[(144\omega_0^2 - \omega^2)^2 + (24\omega_0\omega)^2]}\right\} \qquad \text{(III-17)}$$

Equation (III-17) can be seen to approximate Eq. (III-4) for that range of frequencies for which 12 $\omega_0 > \omega$.

The above mathematical descriptions of the pressure transducer compensation technique are equally valid for any linear, time invariant, second-order dynamic measurement system with an electrical output signal. Also, a single computer compensator stage with the transfer function given by Eq. (III-15) could be used to compensate for any one natural frequency of a multiple-degree-of-freedom system. Several computer compensator stages could be used to compensate for several natural frequencies of a multiple-degree-of-freedom system. As can be seen from Eq. (III-15), the computer circuitry can be programmed to account for the damping characteristics of the pressure transducer. This is a distinct advantage compared with the reaction-force summation technique for situations when the transducer response is damped.

COMPENSATION FOR DYNAMIC STRUCTURAL RESPONSES OF WIND TUNNEL MODEL FORCE MEASUREMENT SYSTEMS

Severe aerodynamic forces imparted to a sting-supported wind tunnel model will excite the natural frequencies of the support sting and the model. The natural-frequency response of the sting can badly distort the force measurement information furnished by the conventional force measurement system which supports the model. To reduce sting vibration distortions, a sting-vibration-compensation system has been developed by personnel of the VKF at the AEDC (Refs. 15 and 16).

A simplified schematic representation of a single-force-component, sting-mounted model is shown in Fig. III-2. From Fig. III-2a (conventional model mounting system) it can be seen that sting motions will introduce compression and/or tension in the load cell spring which will cause a load cell output signal. This sting motion signal will distort the signal caused by aerodynamic forces. To reduce the sting motion distortion, an accelerometer can be attached to the sting, in close proximity to the load cell, as shown in Fig. III-2b. Sting accelerations are then sensed and the accelerometer signal level is properly adjusted and added to the load cell signal. The resultant summed signal is significantly less distorted than the load cell signal, as has been shown under both controlled dynamic conditions and actual test conditions (Refs. 15 and 16).

The preceding compensation procedure has accounted for distortions caused by the excited natural frequencies of the sting. The excited natural frequencies of the model structure may also distort the load cell signal since the sting-vibration-compensation system shown in Fig. III-2 does not compensate for these natural frequencies. Filtering techniques are

often applied to reduce the model natural-frequency distortions. Filter techniques reduce the instantaneous tracking error during periods of natural-frequency "ringing," but increase the tracking error during periods of dynamic change of input force level (such as during force rise time).

When it is desired to minimize the degree of filtering and therefore decrease the tracking error during dynamic-force level changes, the hybrid transducer configuration and compensation circuits may be utilized. This configuration is shown in Fig. III-3. The electronic circuitry to be used is the same as that shown in Fig. 5. The transducer configuration shown in Fig. III-3 is equivalent to that shown in Fig. III-2 insofar as compensation for sting dynamics is concerned, but the Fig. III-3 configuration inherently possesses the additional capability to compensate for one natural frequency of the model and model support structure. Several computer compensation stages in conjunction with the transducer configuration shown in Fig. III-3 would make it possible to compensate for dynamic sting effects, as well as for three or possibly four degrees of freedom of the model and model mount structure.

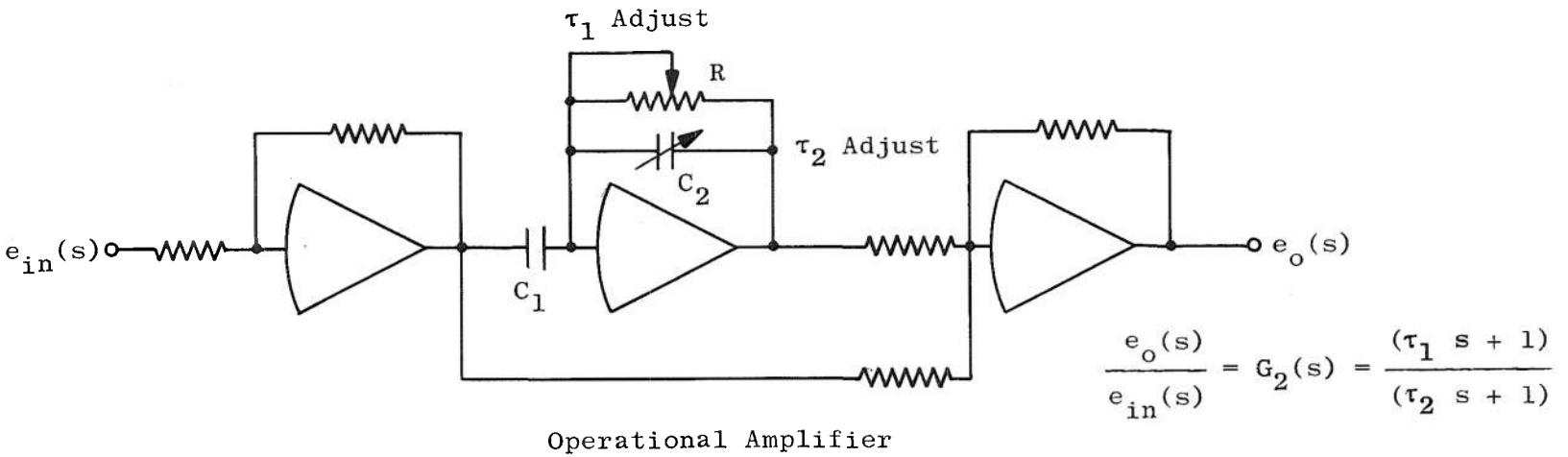

Fig. III-1 Computer Compensator for First-Order Dynamic Measurement Systems

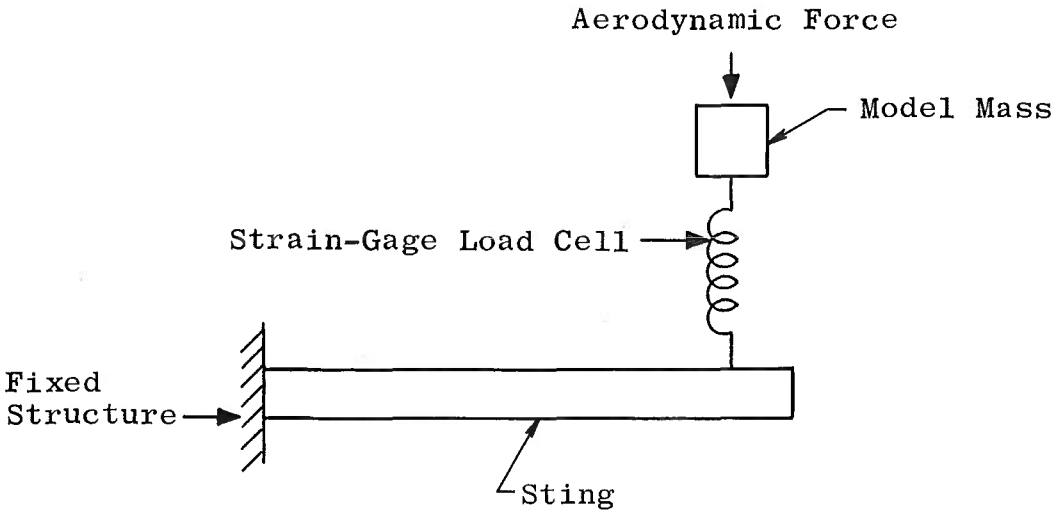

a. Conventional Mounting Configuration

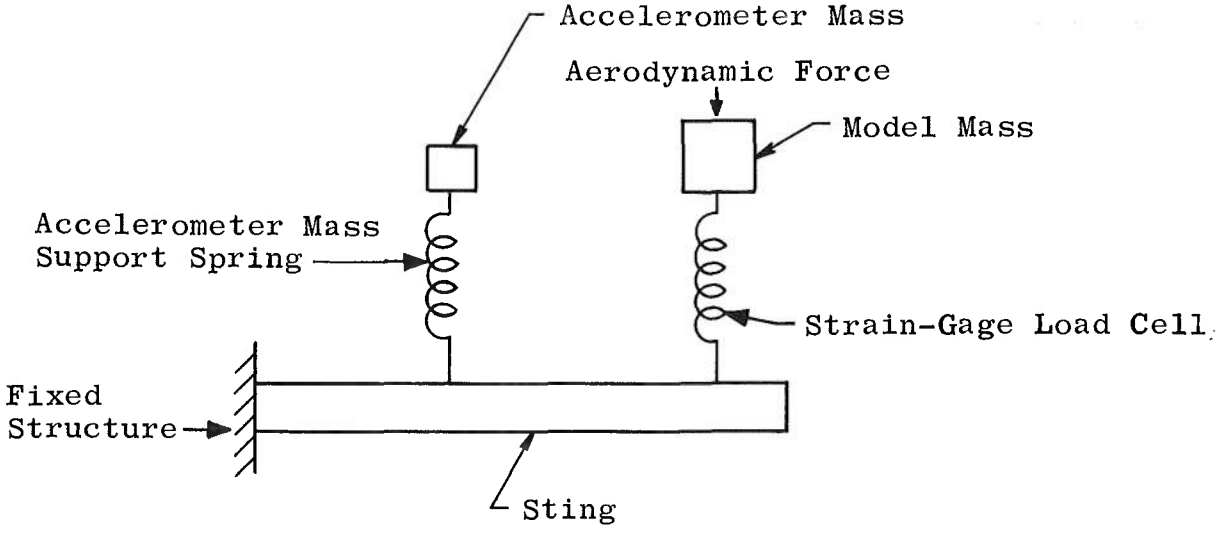

b. Sting-Vibration-Compensation Configuration

Fig. III-2 Schematic Representation of a Sting-Mounted Wind Tunnel Model

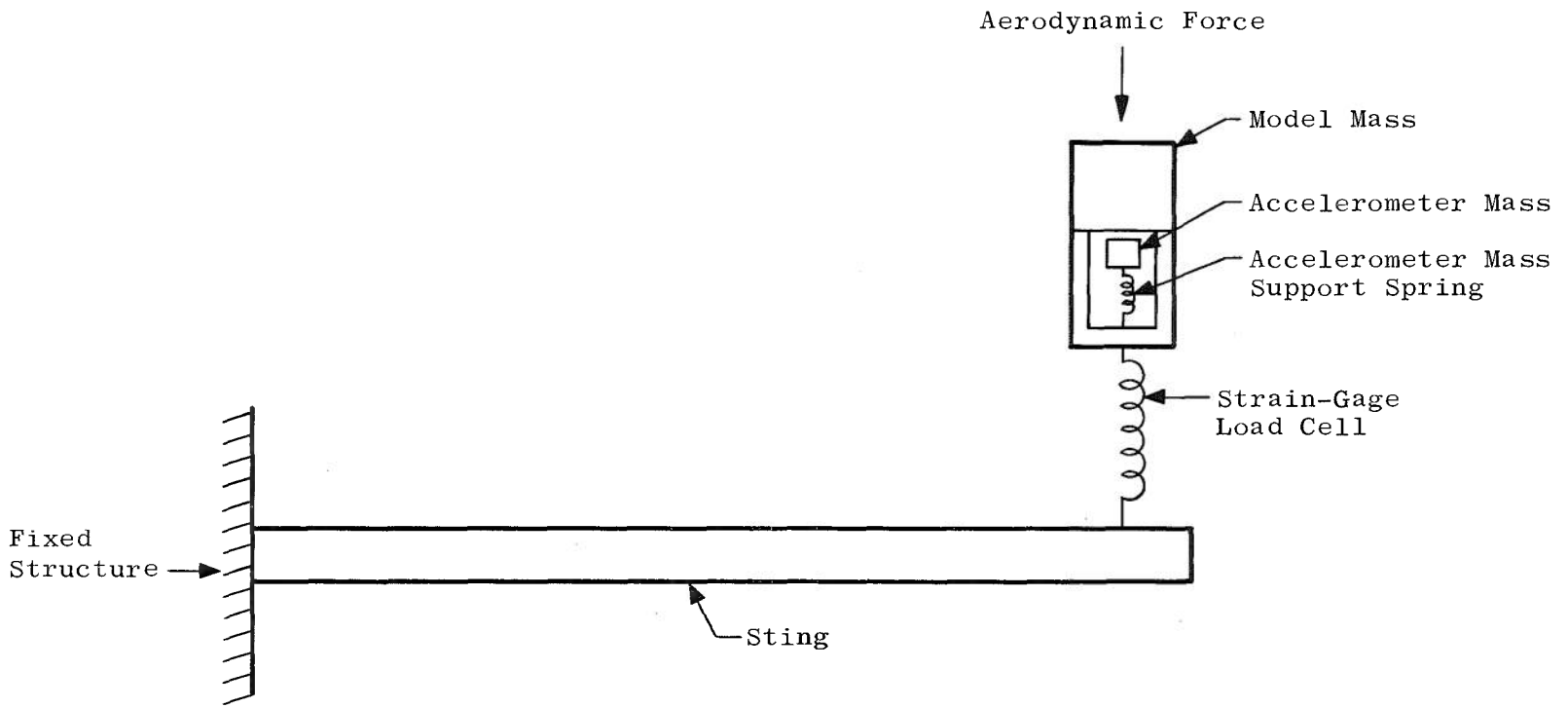

Fig. III-3 Sting-Mounted Wind Tunnel Model - Transducer Configuration for Use of Hybrid Compensation Techniques

UNCLASSIFIED

Security Classification

DOCUMENT CONTROL DATA - R & D

(Security classification of title, body of abstract and indexing annotation must be entered when the overall report is classified)

1. ORIGINATING ACTIVITY *(Corporate author)*
Arnold Engineering Development Center
ARO, Inc., Operating Contractor
Arnold Air Force Station, Tennessee 37389

2a. REPORT SECURITY CLASSIFICATION
UNCLASSIFIED

2b. GROUP
N/A

3. REPORT TITLE
EVALUATION OF A STATIC AND DYNAMIC ROCKET THRUST MEASUREMENT TECHNIQUE

4. DESCRIPTIVE NOTES *(Type of report and inclusive dates)*
Final Report April - June 1967

5. AUTHOR(S) *(First name, middle initial, last name)*
F. L. Crosswy and H. T. Kalb, ARO, Inc.

6. REPORT DATE	7a. TOTAL NO. OF PAGES	7b. NO. OF REFS
September 1968	63	16

8a. CONTRACT OR GRANT NO.
F40600-69-C-0001

b. PROJECT NO.
5730

c. Task 573004

d. Program Element 62302F

9a. ORIGINATOR'S REPORT NUMBER(S)
AEDC-TR-68-117

9b. OTHER REPORT NO(S) *(Any other numbers that may be assigned this report)*
N/A

10. DISTRIBUTION STATEMENT
This document has been approved for public release and sale; its distribution is unlimited.

11. SUPPLEMENTARY NOTES
Available in DDC.

12. SPONSORING MILITARY ACTIVITY
Arnold Engineering Development Center (AETS), Arnold Air Force Station, Tennessee 37389

13. ABSTRACT

This report describes the procedures and results of a critical evaluation of a static and dynamic rocket thrust measurement technique. Two independent dynamic compensation techniques (reaction force summation and computer compensation techniques) were used in a "hybrid" tandem configuration to eliminate force measurement signal distortions caused by the resonant frequencies of the thrust stand. The compensated bandwidth gave a factor of 16 improvement over the conventional load cell force measurement system. With force-time functions simulating a rocket firing, thrust stand natural frequency distortions were eliminated by using the hybrid compensation techniques. The time domain force measurement accuracy using hybrid compensation techniques was shown to be superior to that of the conventional load cell system.

DD FORM 1 NOV 65 1473

UNCLASSIFIED

Security Classification

UNCLASSIFIED
Security Classification

14. KEY WORDS	LINK A		LINK B		LINK C	
	ROLE	WT	ROLE	WT	ROLE	WT
1. thrust stands						
calibration						
force measurements						
2. Rocket thrust stand.						
3. Rocket motors -- Thrust						
4 Thrust -- Measurement.						

16-3

UNCLASSIFIED
Security Classification